E201 242

(2)

PL-TR-92-2158

INVESTIGATIONS OF JOINT SEISMIC AND ELECTROMAGETIC METHODS FOR NUCLEAR TEST MONITORING

Charles B. Archambeau
John B. Davies
Jeffrey Orrey

University of Colorado
Department of Physics/TAGG
Campus Box 583
Boulder, CO 80309

February 15, 1992

Scientific Report No. 1

Approved for public release; distribution unlimited

PHILLIPS LABORATORY
AIR FORCE SYSTEMS COMMAND
HANSCOM AIR FORCE BASE, MASSACHUSETTS 01731-5000

The views and conclusions contained in this document are those of the authors and should not be interpreted as representing the official policies, either expressed or implied, of the Air Force or the U.S. Government.

This technical report has been reviewed and is approved for publication.

JAMES F. LEWKOWICZ
Contract Manager
Solid Earth Geophysics Branch
Earth Sciences Division

JAMES F. LEWKOWICZ
Branch Chief
Solid Earth Geophysics Branch
Earth Sciencs Division

P.P. DONALD H. ECKHARDT, Director
Earth Sciences Division

This document has been reviewed by the ESD Public Affairs Office (PA) and is releasable to the National Technical Information Service (NTIS).

Qualified requestors may obtain additional copies from the Defense Technical Information Center. All others should apply to the National Technical Information Service.

If your address has changed, or if you wish to be removed from the mailing list, or if the addressee is no longer employed by your organization, please notify PL/IMA, Hanscom AFB MA 01731-5000. This will assist us in maintaining a current mailing list.

Do not return copies of this report unless contractual obligations or notices on a specific document requires that it be returned.

REPORT DOCUMENTATION PAGE

Form Approved
OMB No. 0704-0188

1. AGENCY USE ONLY (Leave blank)	2. REPORT DATE	3. REPORT TYPE AND DATES COVERED
	February 15, 1992	Scientific No. 1

4. TITLE AND SUBTITLE

Investigations of Joint Seismic and Electromagnetic Methods for Nuclear Test Monitoring

5. FUNDING NUMBERS

Contract No.
F19628-90-K-0051
PE 62101R
PR 7600
TA 09
WUBJ

6. AUTHOR(S)

Charles B. Archambeau
John B. Davies
Jeffrey Orrey

7. PERFORMING ORGANIZATION NAME(S) AND ADDRESS(ES)

University of Colorado
Dept. of Physics/TAGG
Campus Box 583
Boulder, CO 80309

8. PERFORMING ORGANIZATION REPORT NUMBER

TAGG 001

9. SPONSORING/MONITORING AGENCY NAME(S) AND ADDRESS(ES)

Phillips Laboratory
Hanscom AFB
Massachusetts 01731-5000
Contract Manager: James Lewkowicz/GPEH

10. SPONSORING/MONITORING AGENCY REPORT NUMBER

PL-TR-92-2158

11. SUPPLEMENTARY NOTES

12a. DISTRIBUTION/AVAILABILITY STATEMENT

approved for public release, distribution unlimited

12b. DISTRIBUTION CODE

13. ABSTRACT (*Maximum 200 words*)

This study is designed to develop both linear and non-linear modeling methods for prediction of excitation of atmospheric and seismic disturbances from near surface explosions and earthquake sources in complex media which include strong lateral variability, randomness and non-linear response effects. Comparisons with observations are systematically pursued to evaluate these models and to develop source discrimination methods. In this report we describe examples of non-linear atmospheric excitation by near surface explosions which are carried to ionospheric heights in order to predict fluctuations in ionospheric electron densities and ionization layer positions. These predictions are compared to active EM monitoring by ground stations of ionospheric layer perturbations due to the large amplitude atmospheric waves from surface explosions. We also consider atmospheric turbulent coupling at the earth's free surface and investigate the high frequency seismic noise characteristics resulting from this source using combined seismic and atmospheric modeling. Results are in first order agreement with spectral observations of high frequency noise, in that both the theoretical and observed particle velocity spectra vary as 1/f in the high frequency range from 1 to 50 Hz. Examples of the effects of randomness, large scale lateral variations and near source surface topography on the seismic wave field from near surface explosions are systematically investigated. We find good first order correlations of predictions with the complex regional and near field observations using reasonable structure/topographic models.

14. SUBJECT TERMS

Seismic Waves
Electromagnetic waves
Numerical modeling
Seismic Discrimination
Seismic noise

15. NUMBER OF PAGES

72

16. PRICE CODE

17. SECURITY CLASSIFICATION OF REPORT	18. SECURITY CLASSIFICATION OF THIS PAGE	19. SECURITY CLASSIFICATION OF ABSTRACT	20. LIMITATION OF ABSTRACT
Unclassified	Unclassified	Unclassified	SAR

Investigations of Joint Seismic and Electromagnetic Methods for Nuclear Test Monitoring

Table of Contents

I. Introduction: Objectives and Methods

Objectives

This study is designed to develop both linear and nonlinear wave propagation methods that can model the excitation and propagation of atmospheric and seismic waves from explosion and earthquake sources in realistic, complex media models which include strong lateral variability, randomness and nonlinear response effects.

In modeling the excitation of the atmosphere and ionosphere we include the usual non-linear transport effects as will as ionization in order to infer secondary effects produced by large amplitude neutral wave propagation upward into the ionosphere from a surface or near surface explosion. The overall objectives of the atmospheric-ionospheric modeling are (a.) to predict fluctuations in the electron densities and ionization layer positions in the ionosphere which can be correlated with active EM monitoring by ground stations and (b.) to predict secondary EM field emissions from ion and electron movements induced by the large amplitude atmospheric waves from below. Here the idea is to evaluate and design active and passive EM sensing methods coupled with seismic methods to define a monitoring environment which will allow large industrial explosions to be easily identified based on the strengths and character of the seismic and atmospheric-ionospheric disturbances produced.

The objectives of the seismic wave propagation modeling are to take account of near source non-linear phenomena as well as topographic effects, medium randomness and strong lateral variability in the earth structure, particularly in the crust and upper mantle. We hope to obtain close fits to the complex seismic wave fields observed at regional and teleseismic distances and in so doing, to generate a basis for refined

detection and discrimination of small seismic events.

Basic Concepts and Approach: Electromagnetic Methods

If small nuclear tests are detonated in a decoupling cavity, then their signals in the low frequency range below 5Hz are reduced by nearly two orders of magnitude. In this case the decoupled nuclear explosion produces signals of the same size as common industrial explosions, of which there are many thousands per year in industrial areas. Consequently, it will be necessary to be able to seismically distinguish between these numerous industrial explosions and possible decoupled nuclear tests if a treaty banning such tests were to rely principally on seismic methods for verification. At the present time there is no well documented method for such discrimination, although it is likely that seismic (spectral) methods employing new high frequency (.5 to 50 Hz) seismic detectors, operating with very low internal noise and deployed at depth or as "tight arrays" to reduce high frequency earth noise, will make it possible to distinguish between these types of explosions, as well as between small earthquakes and tamped or decoupled nuclear explosions. In this study we seek to build a firm understanding of the regional seismic wave fields produced by different types of seismic sources in order to properly define discrimination methods and procedures and be able to test and predict their variability and sensitivity in different regional structures.

In addition to seismic methods for event identification, there are other possibilities that are beginning to receive serious consideration. Clearly, sensing of acoustic signals from large industrial explosions is a possible means of identifying these events, since neither nuclear tests nor earthquakes will produce such a large signal in the atmosphere. However, because of signal attenuation and high acoustic noise levels at the

earth's surface, even relatively large acoustic signals from most industrial explosions of interest may not be observable beyond a few hundred kilometers. Nevertheless, acoustic sensors located quite near active mining areas would be useful in identifying the large near surface explosions that are of greatest importance. Since large scale mining areas are relatively rare, one would need to monitor only a few areas using this method to achieve nearly total monitoring coverage of the largest industrial explosions. Consequently locally distributed acoustic sensor arrays around major mining areas can provide critical data for monitoring, particularly when coupled with similar seismic monitoring arrays.

Since even small industrial explosions at normal mining depths will produce a much larger signal in the atmosphere than a decoupled or tamped nuclear test, it is possible that the existance of this large signal difference could be used in other ways, besides direct acoustic field measurents, to help identify these sources. That is, while even the larger acoustic signals will be small relative to noise after propagation over a few hundred kilometers in the atmosphere near the earth's surface, this is not the case for the acoustic wave field propagated directly upward into the upper atmosphere and ionosphere. In this case the fact that the air density decreases rapidly with altitude causes the amplitude of an acoustic wave to increase rapidly with increasing height and to strongly perturb the ionosphere over an area of the order of 100 kilometers in radius around the source epicenter. Consequently, remote EM sensing of the ionosphere using radio frequency transmitter - receiver systems can detect ionospheric perturbations due to the acoustic waves from industrial explosions. Observationally the acoustic waves produce ionospheric boundary motions resulting in doppler shifts in the reflected EM signals recorded on the ground. By placing radio frequency receivers

and transmitters in a distributed network, comparable to an in - country seismic monitoring network of about 30 stations, it appears possible to provide complete monitoring capability on a continental scale. In principal it should be possible to identify large industrial explosions with high probability due to the EM signal shifts observed. Coupled with seismic monitoring then, the occurrence of an event that had an explosive seismic signature, but that produced no ionospheric EM effect, would indicate a probable decoupled or tamped nuclear test.

Besides the possibility of active monitoring of the strong perturbations in the reflecting layers of the ionosphere by radio frequency sounding, it is possible to detect secondary EM emissions from the ionosphere. Thus, passive electromagnetic monitoring of the electromagnetic environment, particularly at low radio frequencies, offers yet another opportunity to address source identification and discrimination issues.

As a consequence of these possibilities, we focus on modeling the atmospheric and ionospheric disturbances produced by near surface explosions of various types in order to provide an understanding and quantitative prediction of the magnitude and character of these effects. Based at least partly on such results, we can then hope to define and test particular methods of acoustic and EM monitoring that can be effective.

Basic Concepts and Approach: Seismic Methods

The seismic discrimination approach envisioned is to make use of the enriched high frequency content of seismic waves radiated by decoupled and tamped nuclear explosions as compared to earthquakes and large industrial explosions. Here the idea is that earthquakes, producing the same low frequency compressional signal level as (say) a decoupled nuclear explosion, will produce lower levels of high frequency

compressional wave energy and so the ratio of high frequency compressional (P) wave energy to low frequency P wave energy will be different for the two source types. Physically this occurs because the source dimension of the comparable earthquake is much larger than that for the explosion and, further, because the energy release process is fundamentally different. (This is discussed in detail by Evernden, Archambeau and Cranswick, Rev. of Geophysics, 1986).

On the other hand, while a decoupled nuclear explosion and a large industrial explosion release energy from roughly comparable volumes, the nonlinear effects within the source volume are expected to be sufficiently different to allow discrimination using compressional wave spectral differences of the same sort that are used to discriminate nuclear tests and earthquakes.

In this regard, industrial explosions are distributed spatially, with partial charges typically in bore holes with regular spacing (tens of meters intervals) and often detonated with time delays between the firing of individual charges. This is done to avoid massive localized surface rupture and "blow-out" and also to enhance fracturing of the material over the largest possible volume using the smallest total amount of charge. As one important consequence, the time-space separation of the charges will result in nonlinear constructive interference† of the shock waves from the individual charges. This interference results in maximum localized over - pressures and very efficient fracturing of the material. When viewed as a seismic source, that is as a radiator of far-field elastic waves, such a source expends a larger proportion of it's total energy in fracturing the surrounding material than would the same total charge

† Interacting shock waves will form "Mach Stems" corresponding to a moving plane of shock intersection, where the pressure jump is significantly larger than either of the pressure jumps along the individual shock fronts.

detonated in a single small volume within the medium. Compared to a tamped nuclear explosion, or to a decoupled nuclear test, the amount of energy radiated as seismic waves should be significantly lower when normalized for yield. More specifically, the microfracturing produced should greatly reduce the high frequency energy available to be radiated from a spatially distributed industrial explosion, so that one would expect the radiated seismic wave to be depleted in high frequency spectral content compared to that from a comparable spatially concentrated explosion. Therefore, the directly radiated compressional (P) wave from a large industrial explosion should appear earthquake-like, that is reduced in high frequency amplitude, relative to comparable nuclear tests of either the tamped or decoupled types.

Joint Seismic, Acoustic and Electromagnetic Discrimination Approach

The use of both the EM and seismic methods together to identify seismic sources is summarized in Table 1. Here, in the column on the left, we compare the expected signal levels (relative to noise) for seismic, acoustic and EM field detections from different source types listed in the row along the top.

Multiple Field Discrimination of Small Seismic Events
A List of Expected Qualitative Differences

Discriminatory Signal Type	Small (m_b < 4) Event Types, all with the same "low" frequency seismic P wave Amplitude			
	Tamped Nuclear Test	Decoupled Nuclear Test	Industrial Explosion	Shallow Earthquake
Regional High Frequency (f > 10) Seismic P wave Signal (Relative amplitude)	Moderate / Large	Large	Small / Moderate	Small
Near - Regional Acoustic Signal (Relative amplitude)	Small / Undetectible	Undetectible	Large	Undetectible
Ionospheric E-M Sounding (Relative amplitude)	Small	Undetectible	Large	Small / Undetectible
Secondary Ionospheric E-M Emissions (Relative amplitude)	Small	Undetectible	Large	Small / Undetectible
	signature: M/L, S/U, S, S	signature: L, U, U, U	signature: S/M, L, L, L	signature: S, U, S/U, S/U

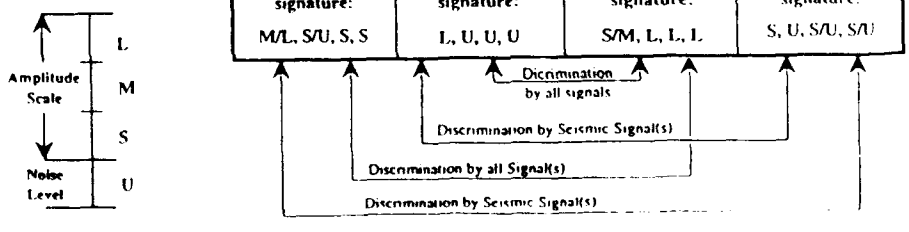

These event types are comparable in that they are chosen to have the same low frequency (f < 1Hz) P wave signal level. (That is they are chosen to have the same standard m_b value.) For such a set of "normalized" event types we list the signal levels, in qualitative terms, to be expected for each of the signal types, in the table entries. These provide an expected "signature" for each of the event types. The method of discrimination of the events is then indicated by the arrows showing what comparisons could be made between "signatures" to identify the events.

In the following sections we describe current results involving both observational studies and theoretical modeling studies of the physical phenomena underlying these discrimination methods.

II. High Frequency Seismic Signal Detection and Spectral Discrimination: Observations

Spectral discrimination has been tested in the past (*eg.* Savino *et. al.*, 1980) and found to be effective for events of magnitude larger than about 3.5 to 4.0. These tests were conducted using relatively low frequencies (*ie.* using P wave magnitudes measured at about .3 Hz versus those at about 3.5 Hz.) The method was termed a "Variable Frequency Magnitude" method or "VFM" method. Figure 1 shows an example of single station discrimination in the far regional distance range. This method has been proposed by Evernden *et. al.* (1986) for the discrimination of small events, in the range $m_b \approx 2$ to $m_b \approx 4$, at regional distances. This requires measurement of high frequency data in the band from about 1 Hz out to 25-30 Hz. Based on preliminary observations of high frequency P wave data in the near regional distance range it was inferred that such a high frequency band could be obtained at stations in *stable*

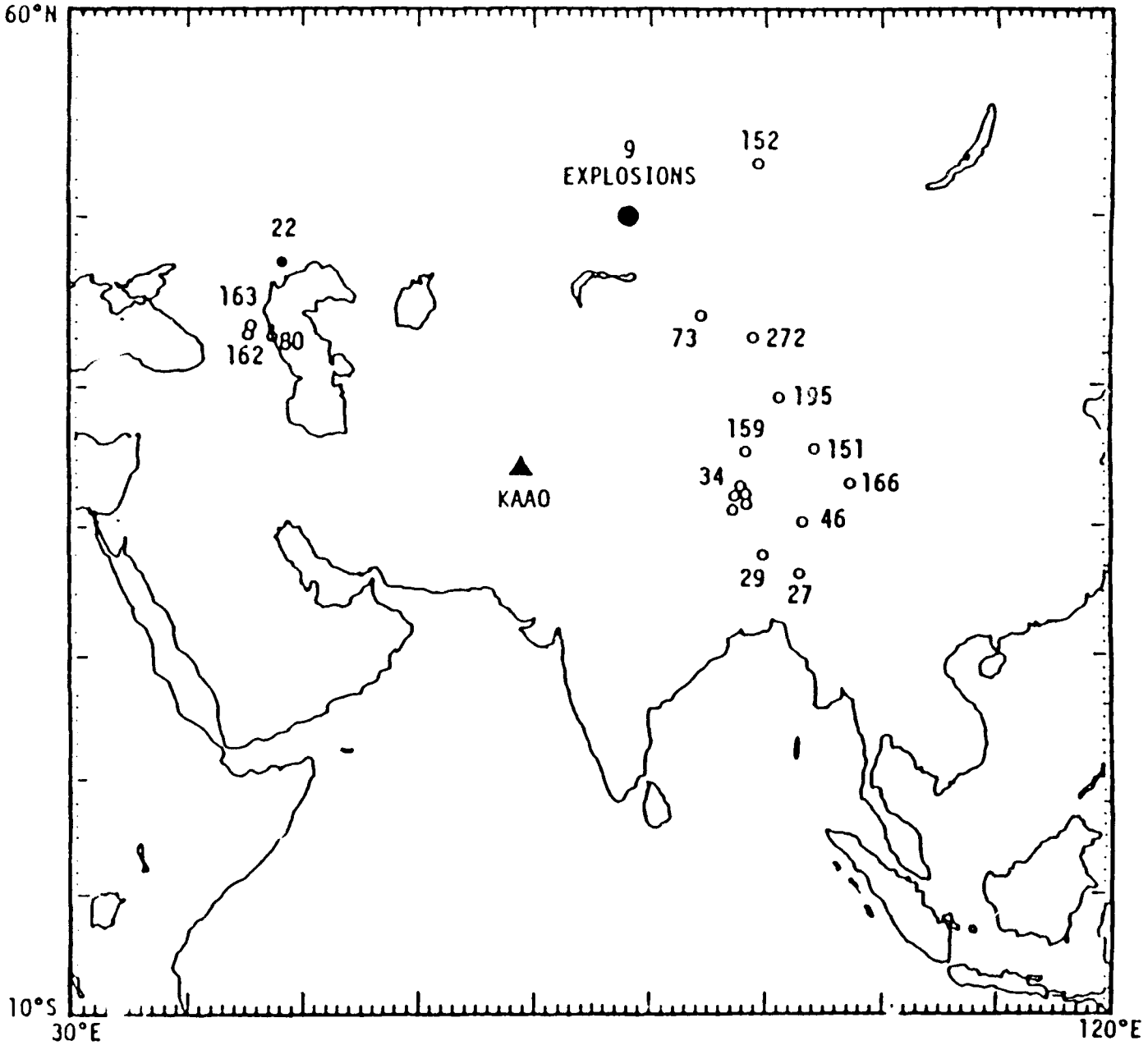

Figure (1a). Distribution of events from the Eurasian data set in the regional distance range from the station KAAO at Kabul, Afghanistan (solid triangle on map.) The solid circles denote events identified as nuclear explosions based on VFM results from KAAO and other stations in the detection network. (Savino *et. al.*, 1980.)

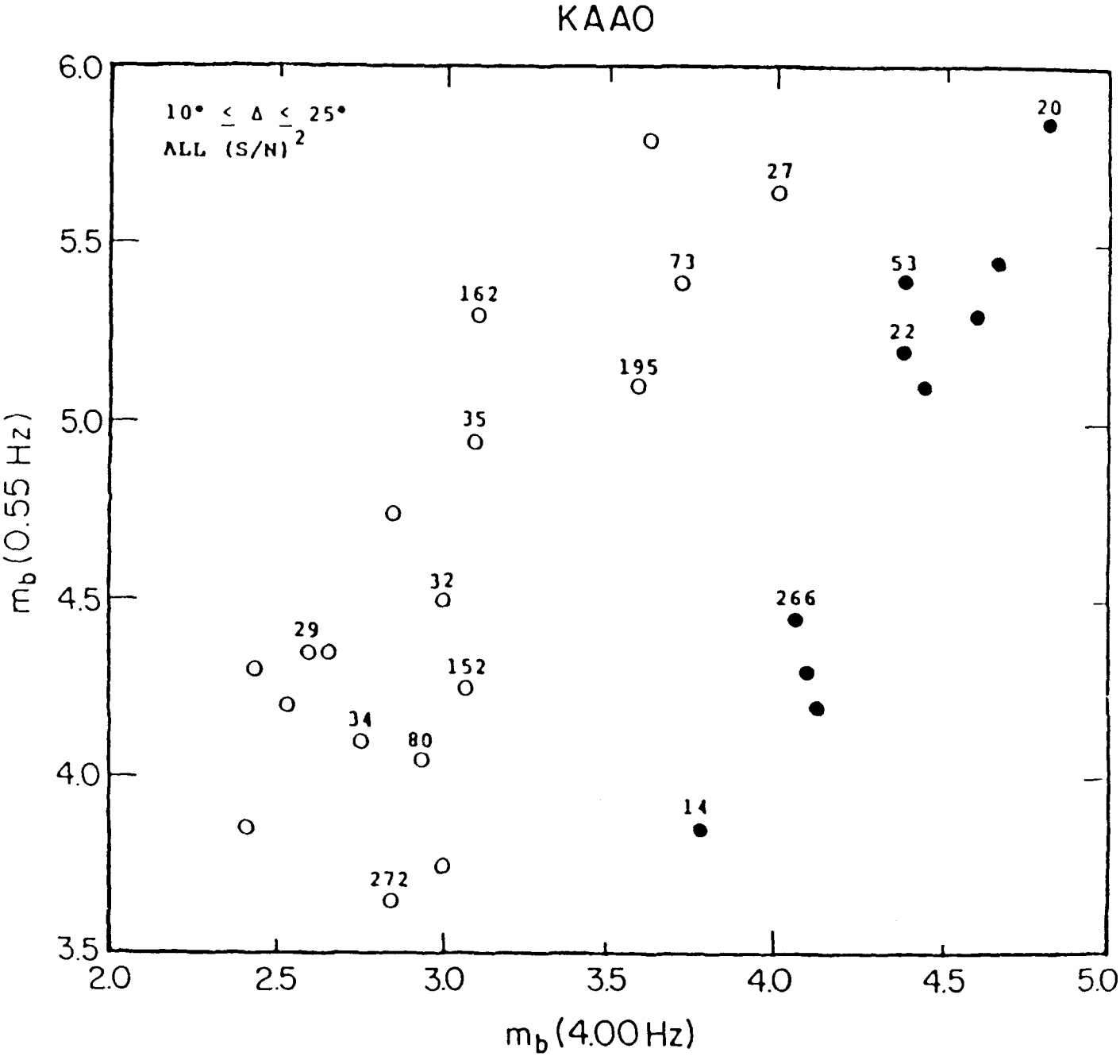

Figure (16). Regional VFM results obtained at the station KAAO for the event set indicated in Figure (23). The event magnitudes range from somewhat more than $m_b = 3.5$ to somewhat less than $m_b = 6.0$. The separation of nuclear explosions and earthquakes is of the order of .75 magnitude units. Nine of ten explosions were tests at the Kazakh test site while one was at the north end of the Caspian sea (No. 22). All the explosions and earthquakes had similar propagation paths to the detecting station so that the differences in VFM results are not likely to be due to path differences between the two classes of events. The differences are, therefore, likely to be true measures of basic spectral differences in the compressional waves radiated by the two source types. (Savino *et al.*, 1980.)

continental areas out to about 1000 km. and in tectonic areas to around 300-400 km.

Data obtained from the (former) Soviet Union near the Kazakh test site showed encouraging results. In particular, high frequency signals from chemical explosions ($m_b \approx 2$) were well recorded at distances as large as 640 km. (The maximum distance of recording.) Figure 2 shows an example recorded at a station (KSU) with noise characteristics that were not particularly good. (Better results could be expected at a relocated site in the same area.) In any case, the spectral range for the P wave signal with S/N > 1 was from about .7 to 28 Hz.

Data from other explosions (nuclear and chemical) were also observed and some characteristics were summarized by Givens *et. al.* (1989), as shown in Figure 3. The data came from stations involving both tectonic and stable continental paths, so that there is scatter in the distance trends of the high frequency "cut-off" for this reason. In addition, the yields of the various explosions were very different. Nevertheless there were indications that one can expect to observe 30 Hz P wave signal at distances of from 700 to 1000 km. from explosion sources as small as 10 tons, and to 20 Hz at distances of the order of about 1200 km., for paths in stable continental areas.

Our recent results, relating to the efficiency and nature of very high frequency P wave propagation in tectonic and stable continental areas, suggest that previous inferences by Evernden *et. al.* (1986) were too crude and did not properly characterize the high frequency P wave signal propagation. In these estimates the approximation for the ratio of P wave spectra at two distances Δ and Δ_0 is given by (for P_n or P):

$$A(\omega, \Delta)/A_0(\omega, \Delta_0) = (\Delta_0/\Delta)^m exp[-\frac{\pi f}{Q_p V_p}(\Delta - \Delta_0)]$$

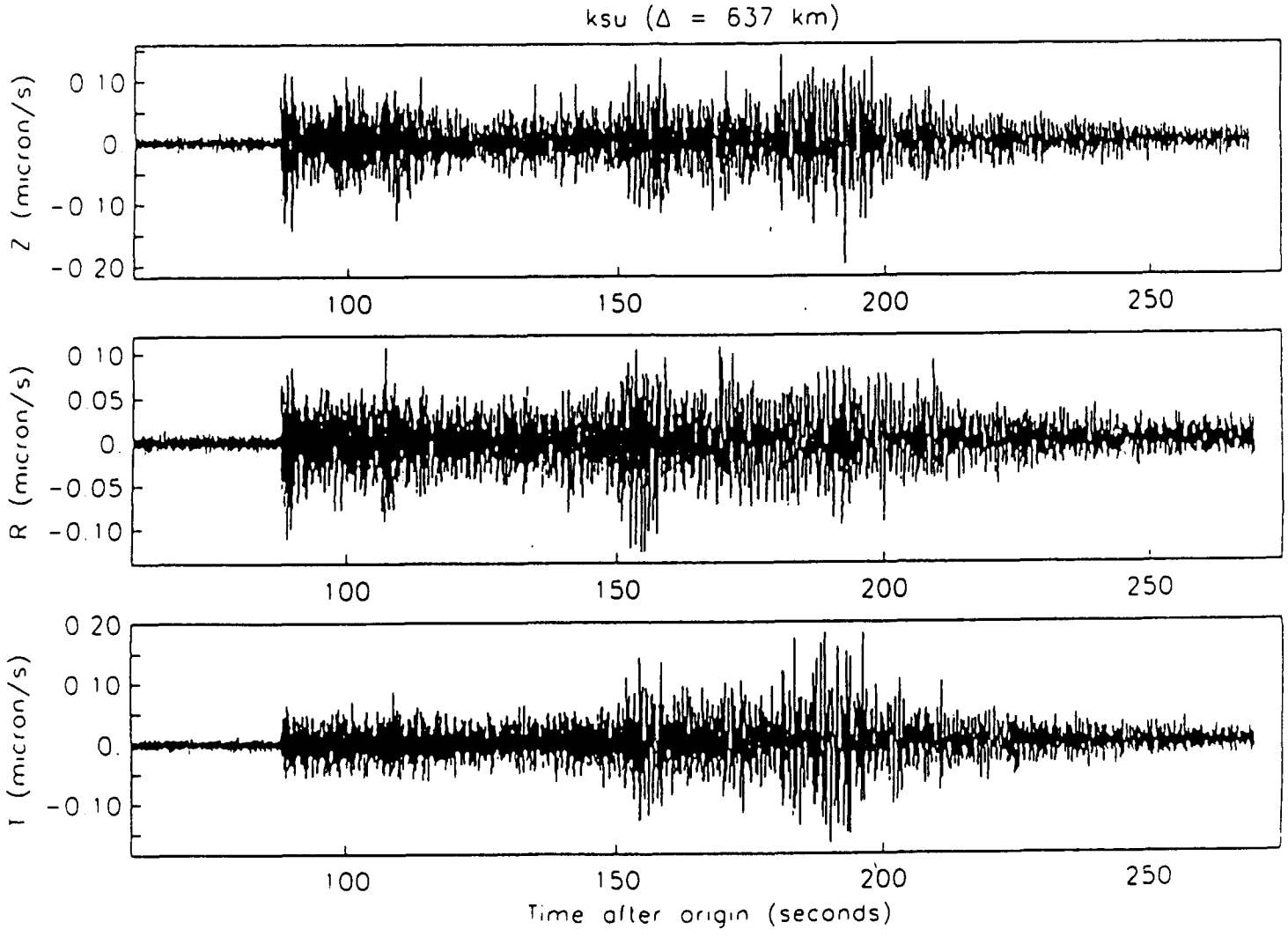

Figure 2-a. Seismograms of components of ground motion recorded at a distance of 637 km. from a 10 ton chemical explosion in the area of the nuclear test site near Semipalatensk in Kazakhstan.

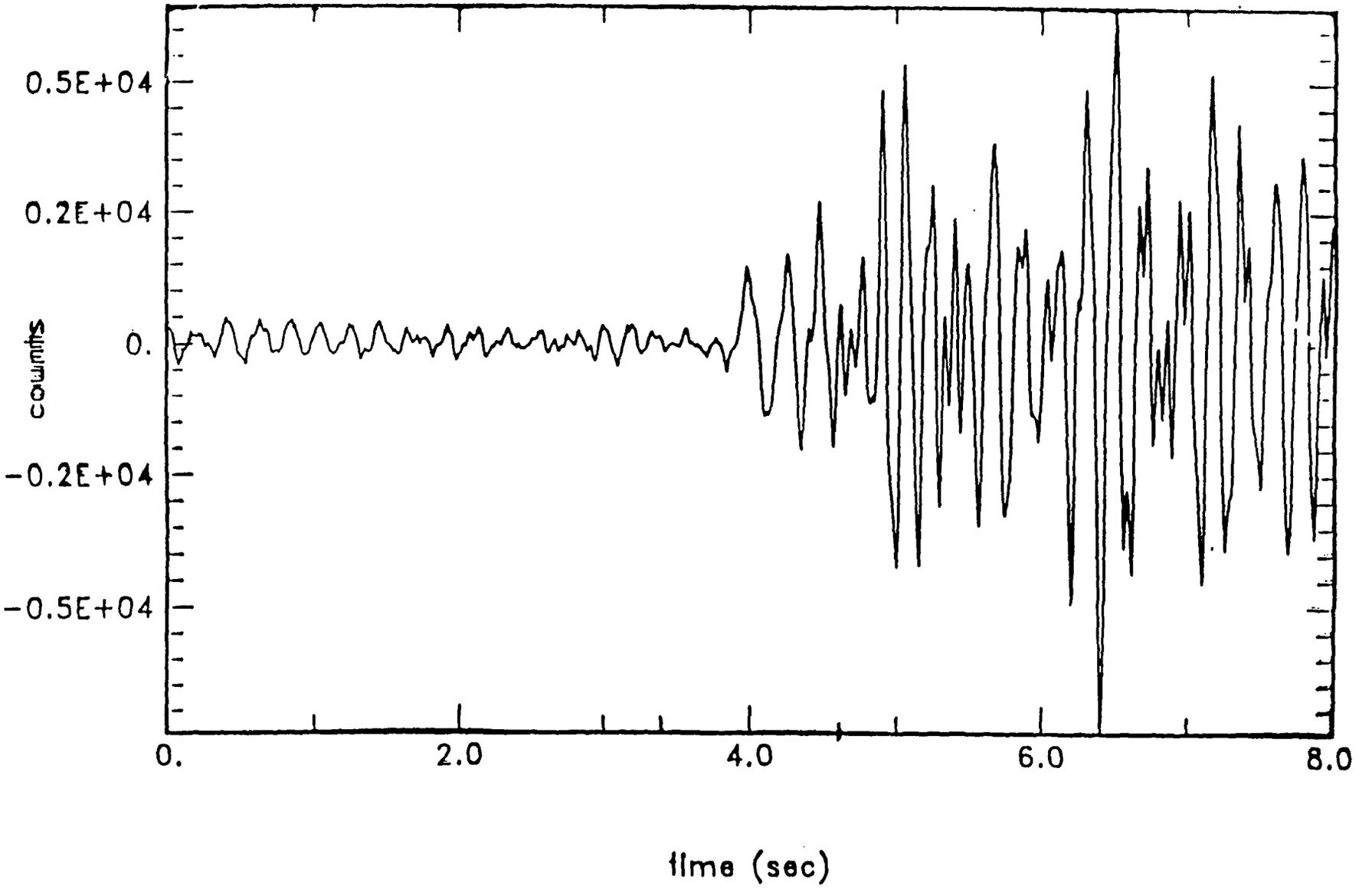

Fig. (2b): Recording of vertical component of ground motion from a 10 ton chemical explosion at a distance of 650 km, in the area of the Kazakh test site, USSR. (From NRDC-Soviet Academy Nuclear Test Monitoring Program, Sept. 1987.)

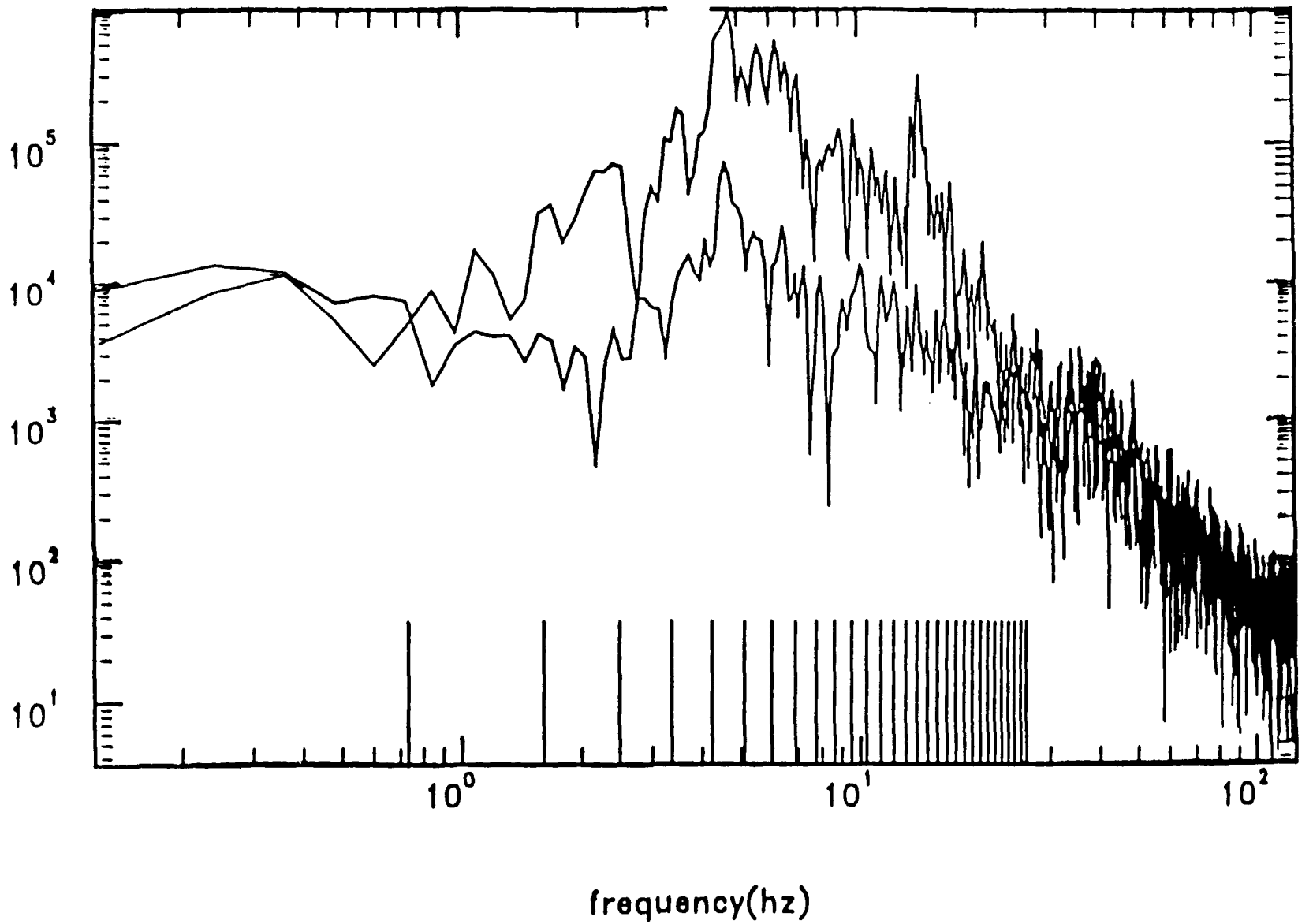

Figure (2c): Raw (uncorrected for system response) spectra of 4 seconds of signal and noise from the ten ton chemical explosion shown in Fig.(2b), at a distance of 650 km., recorded in the area of the Kazakh Test Site, USSR. The lines on the frequency scale at the bottom indicate (equally spaced) frequency samples in the spectral range where the signal to noise ratio is greater than unity. (This band is from about .7 HZ to 28 HZ.)

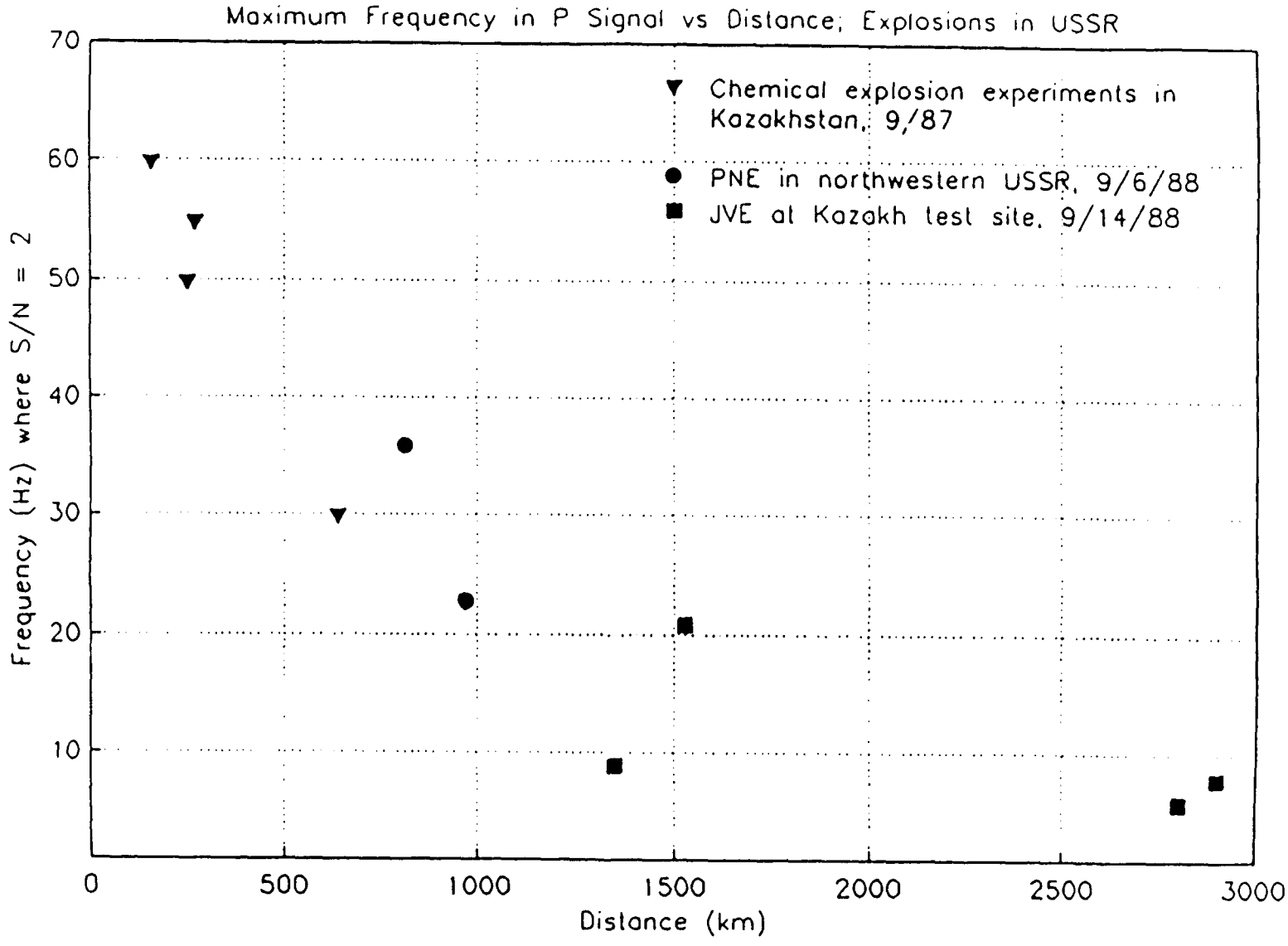

Figure (3). **Maximum measurable frequency (S/N > 2) in P wave signals versus distance for various sized explosions (From Givens *et. al.*, 1989).**

with Δ denoting epicentral distance and Q_p and V_p being the path averaged dissipation function and average compressional velocity respectively. The geometric exponent factor, m, is two for P_n in a very simple layered geometry, but in general can be expected to be in the range from about 1/2 to 3 in complex structures. An approximate form adopted for $Q_p(f)$ in the high frequency range is:

$$Q_p(f) = Q_O f^{\alpha}$$

In the study by Evernden *et. al.* 1986 a geometric fall-off varying inversely with the square of distance was used and a very high P wave Q, in the range near 9000, was inferred from eastern U.S. data. This was used as a standard for stable continental P wave propagation, that is "P_n", in the regional distance range. However, results from USSR studies of JVE data show that the geometric effect is closer to an exponent dependence of -1 on distance, or even -.75 on some paths, and that the Q for "P_n" is in the range from to 3000 to 4000 in stable areas, These results are illustrated in Figure 4 where the best fits to the amplitude ratio data from the JVE event is given by geometric spreading exponents (m) near 1. The geometric exponent for tectonic areas is, on the other hand, closer to 2 while the Q value turns out to be in the range from 1000 to 2000, and typically higher than the 1000 value used by Evernden *et.al.* This is illustrated by the results in Figure 5.

The net result is that we may be able to expect detection capability of very high frequency P waves out to the distances used by Evernden *et. al.*, but the propagation characteristics are actually somewhat different than those inferred by them. Nevertheless, spectral discrimination at regional distances should be possible to $m_b \approx 2$ for different kinds of explosions and earthquakes.

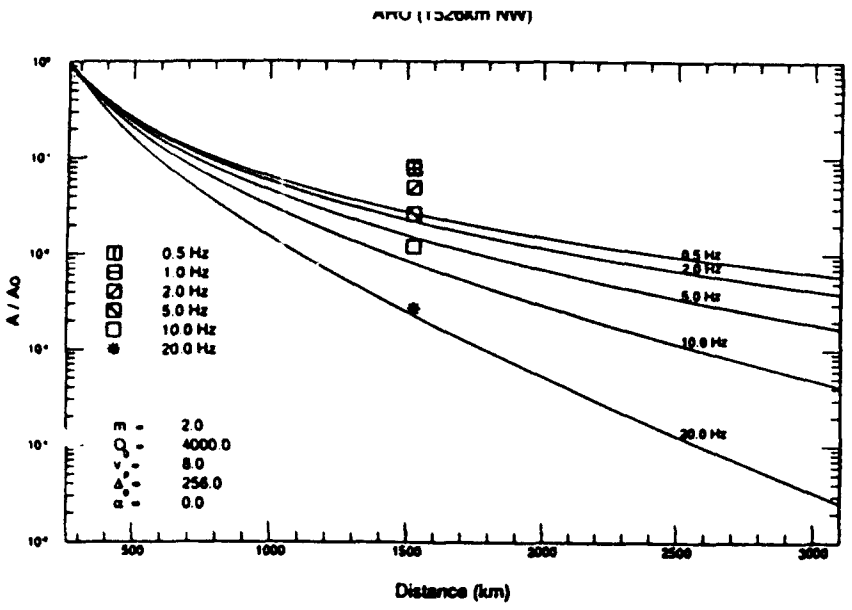

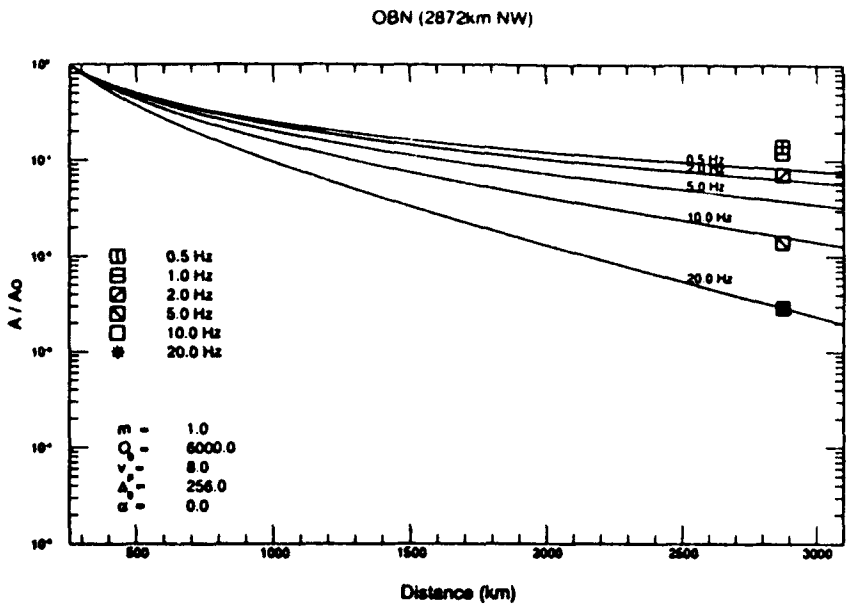

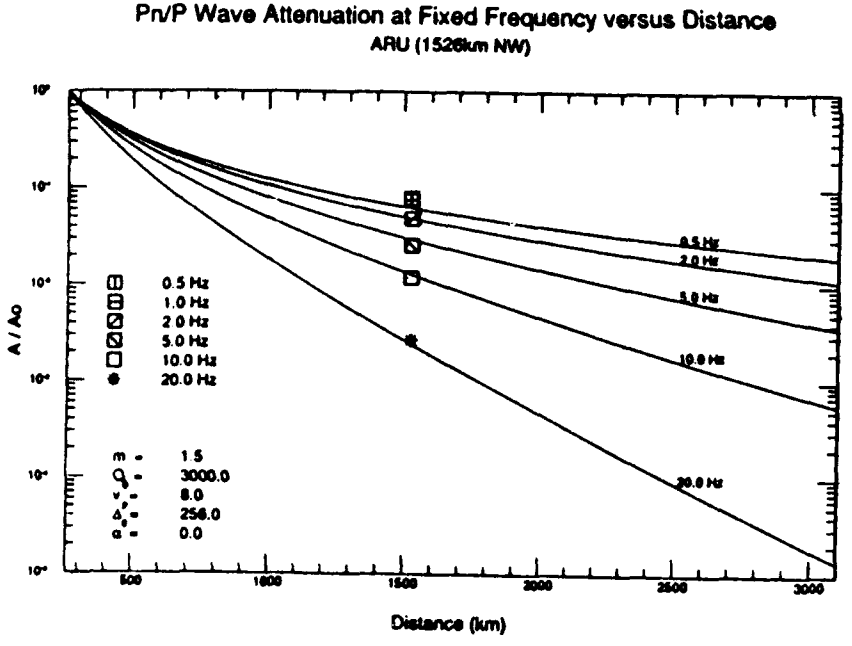

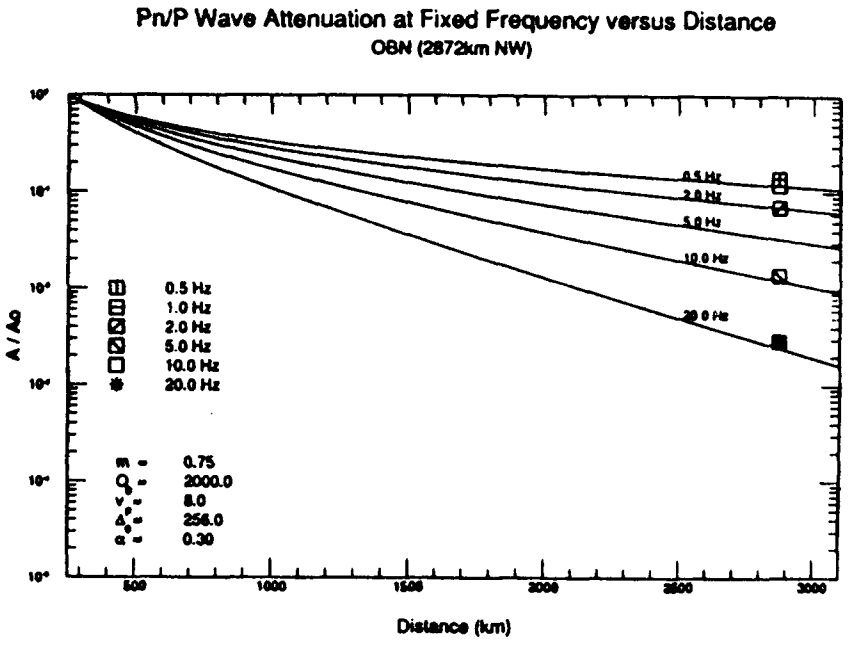

Figure (4) Fits of observed spectral ratios of P_n and P from the JVE at ARU (Arti, U.S.S.R) and OBN (Obninsk, U.S.S.R.) normalized by the P_n spectra at MSD (Bayanaul, U.S.S.R.) near the Soviet test site. A better fit to the P_n ratio at ARU is obtained by reducing the spreading exponent m to 1.5. At OBN the data shows scatter, but the spreading exponent is clearly less than 1. A best fit is obtained for a mildly frequency dependent Q_p. Both paths are in a stable continental area and the mean Q_p values are quite high at high frequencies.

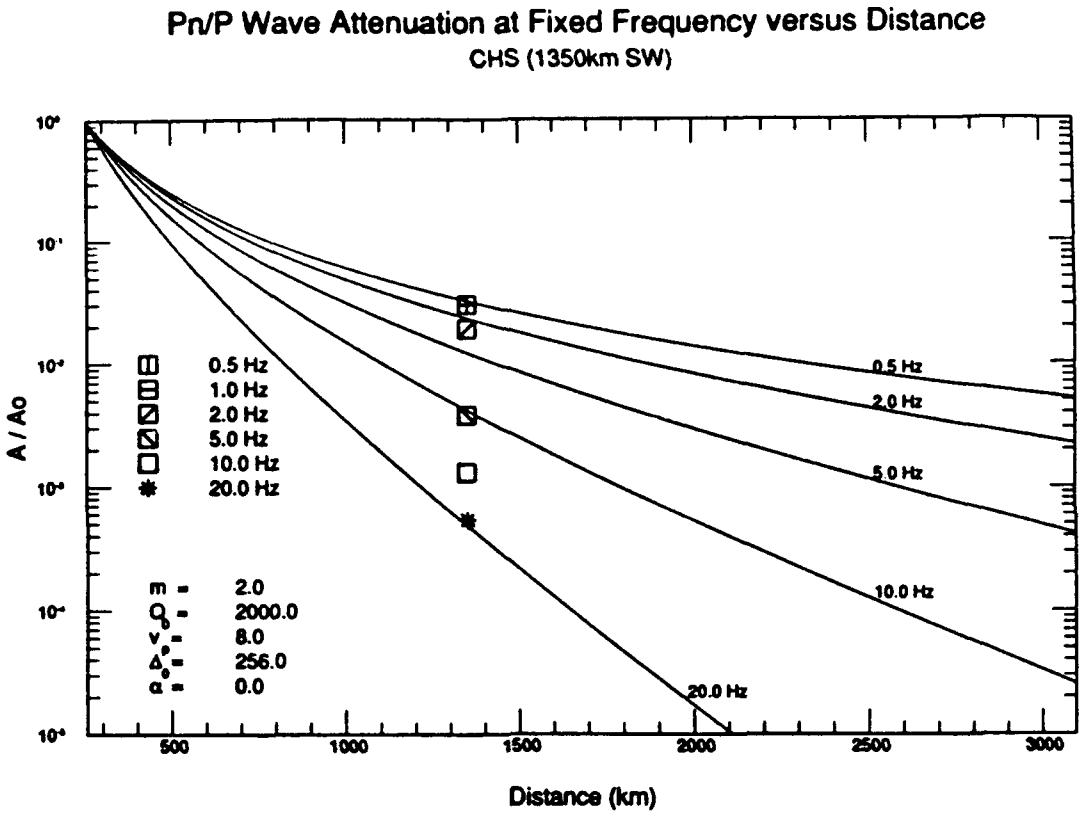

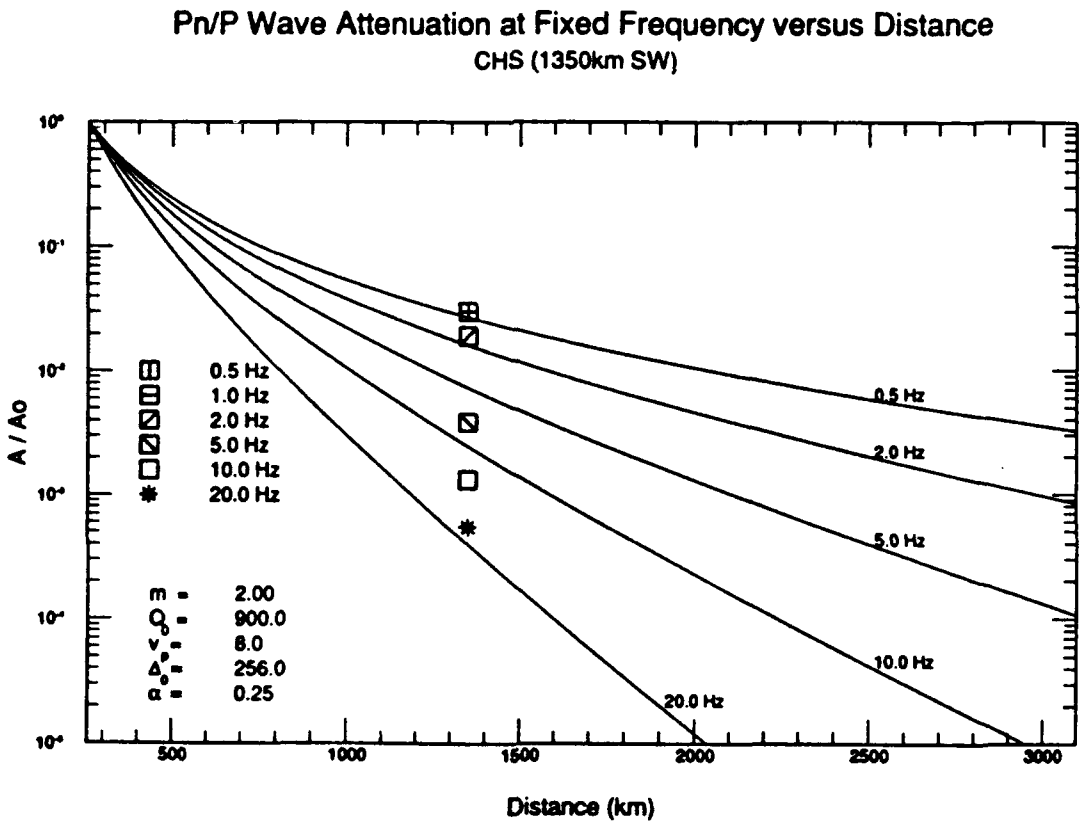

Figure 5 Theoretical fits to spectra ratio data for P_n between the station CHS near Garm and a temporary station near the Soviet Kazakh test site.

We conclude that on the basis of these observations the predictions of regional discrimination by VFM methods should be effective to $m_b \approx 2$ at distances of the order of 1000 km in stable continental areas. Station distances would have to be lower in tectonic areas, around 500km, to achieve such low magnitude identification capability, but since such areas are limited globally this does not imply that extremely large numbers of stations would be required for coverage. Indeed, the station distributions for monitoring a land mass as large as the former Soviet Union would be about the same as that estimated by Evernden *et. al.* (1986).

III. Modeling High Frequency Seismic Signal Propagation

Evaluation of various computational methods for seismic wave field propagation has been the first objective of this part of our investigations. Useful techniques include standard finite difference, finite element, and pseudospectral methods. While standard finite difference and finite element techniques allow straightforward and reasonably accurate treatment of free surface and absorbing boundary conditions on computational grid edges, they are prohibitively expensive for application to wave propagation to regional distances and up to the frequencies of interest. A typical second order finite difference method requires a computational grid fine enough to sample the smallest wavelength disturbance with 8 or 10 grid points in order to avoid numerical dispersion and consequently results in a very large computer memory requirement and, as well, long computational times.

The primary advantages of a pseudospectral method are reduced core memory requirements, faster run times, and improved accuracy for solutions containing large gradients. Because the method may require only 2 or 3 computational grid points per

smallest wavelength to avoid numerical dispersion, it can be up to 25 times as efficient as a second order finite difference solution of equal accuracy for 2-dimensional problems. The actual sampling requirements depends on the variations of the material structure.

The Pseudospectral Method

For our purposes, a pseudospectral method refers to solution of a partial differential equation by employing spectral estimation of the spatial dependencies and finite differencing in time. Spatial differentiation is performed in the spectral domain and then transformed back to the spatial domain. Typically the field variables' spatial dependence is expanded in a Fourier basis, so that use can be made of efficient Fast Fourier Transforms in obtaining a spectral representation.

Consider a first-order spatial derivative of a field variable p in one dimension, x: $\frac{\partial}{\partial x} p\ (x,t)$ is evaluated by applying a spatial Fourier transform to p(x,t) at discrete locations corresponding to computational grid points in the x-direction. After multiplying the transformed quantity $\tilde{p}\ (k_n,t)$ by wave-numbers ik_n, n = 1,..., N, where N is the number of grid points in the x-direction, the derivative is obtained by performing the inverse tranform. For mixed partial derivatives, e.g. $\frac{\partial^2}{\partial x \partial y} p(x,y,t)$, the process is repeated along the other dimension.

By expanding the dependent variables' spatial dependence in a trigonometric basis, optimal grid-point per wavelength sampling is attained. The Nyquist criterion indicates that theoretically only two gridpoints are required per minimum wavelength within the grid. One may view the pseudospectral method as either the trigonometric

interpolation of the derivative of a function or as a finite difference algorithm of maximum order, where all neighboring grid points along one grid dimension are used in the local computation of the derivative. The two interpretations are equivalent.

For a linearly elastic, heterogeneous medium, we formulate the equations for particle motions as

$$\dot{pv}_i = \tau_{ij,j} + pf_i \tag{1}$$

and

$$\dot{\tau}_{ij} = \lambda v_{k,k}\delta_{ij} + \mu(v_{i,j} + v_{j,i}), \tag{2}$$

where p, λ, and μ are the position-dependent density and elastic constants of the medium, and v_i and τ_{ij} denote particle velocities and stresses beyond the equilibrium configuration. Dots indicate time derivatives, and commas between indices denote partial differentiation with respect to the spatial coordinate labeled by the index following the comma. δ_{ij} is the Kronecker delta function and f_i corresponds to body force components. Equations 1 and 2 are solved by a pseudospectral method, and appropriate boundary conditions must be applied. Treating the stress tensor explicitly allows for incorporation of anelastic rheologies and explicit specification of a free surface boundary condition on one side of the grid. The periodic nature of the boundaries of a Fourier pseudospectral formulation prohibit the use of absorbing boundary conditions on the other sides, so damping must be used along grid boundaries to avoid reflections.

Because the accuracy of the pseudospectral method surpasses that of a lower-order differencing scheme, it is comparatively more useful for approximating solutions that contain large gradients or discontinuities. Nevertheless, large gradients or discon-

tinuities in the true solution cause Nyquist spatial wavenumber contamination of the pseudospectral solution. At the Nyquist frequency the spectrum of a real-valued space variable should have no imaginary component. However, the phase shift introduced by the first-order derivative operator ik causes imaginary contributions at the Nyquist frequency, effectively violating the FFT's assumptions of symmetry and real-valued input. This error is particularly serious for the modelling of surface and interface waves, which propagate along discontinuities. In order to accurately determine the effects of lateral variations in material structure on surface wave phases, it is important to resolve or at least minimize this error.

The Chebychev Expansion Method

Some authors have eliminated the Nyquist error by formulating equations 1 and 2 with the field variables and material parameters staggered within each computational grid cell (Witte and Richards, 1990). In a pseudospectral method, the relative space between the location at which variables are evaluated adds a phase shift to each variable in the spectral domain, effectively concelling the phase shift due to the derivative operator and ensuring no imaginary components at Nyquist frequency. We have found such formulations to be accurate for body wave calculations, but surface waves develop a well-known ringing as the solution is integrated in time. The staggered-grid formulation appears to make this problem worse.

Other authors have successfully eliminated surface wave ringing by choosing a computational grid with the spacing reduced near the free surface. In particular, one choice is a grid whose spacing with depth corresponds to the zeroes of Chebychev polynomials of increasing order. The use of this functional form is desirable in that

the Chebychev basis can be expressed in terms of trigonometric functions, retaining the use of Fast Fourier Transforms in the solution (Kosloff, et. al. 1990). The finer grid spacing makes available higher wave-numbers for synthesizing the wavefield in the vicinity of the free-surface discontinuity, and the non-periodic nature of the basis allows the use of absorbing boundary conditions on the opposite end of the grid.

In Figure 6 we compare the analytic solution of Lamb's problem to that of the Chebychev method for a vertical vector surface source with a maximum frequency content of 1 Hz. The material paramenters correspond to a compressional velocity of 5.4 km/s, a shear velocity of 3.1km/s, and a density of $2.5 g/cm^3$. The grid is scaled so that the grid points in the vicinity of the free surface sample between 10 and 30 times per wavelength. The numerical solution compares well to the exact analytic result.

The primary disadvantage to the Chebychev basis method is that a stable solution requires a fourth-order Runge-Kutta method for integration in time. This makes the algorithm slow. We are presently looking into other time-integration schemes for the Chebychev method, in addition to alternative solution techniques on a regular grid.

The Complex Pseudospectral Method

As an alternative technique for avoiding the Nyquist error, we have chosen to solve the equations of motion on a non-staggered grid but now define each field variable to be complex. Solving for both real and imaginary components at each time step preserves all phase information and circumvents the Nyquist noise problem in the same manner as does the staggered-grid technique.

Figure 7 shows the Rayleigh wave produced from Lamb's problem using a complex-field pseudospectral method and the same material parameters and source as

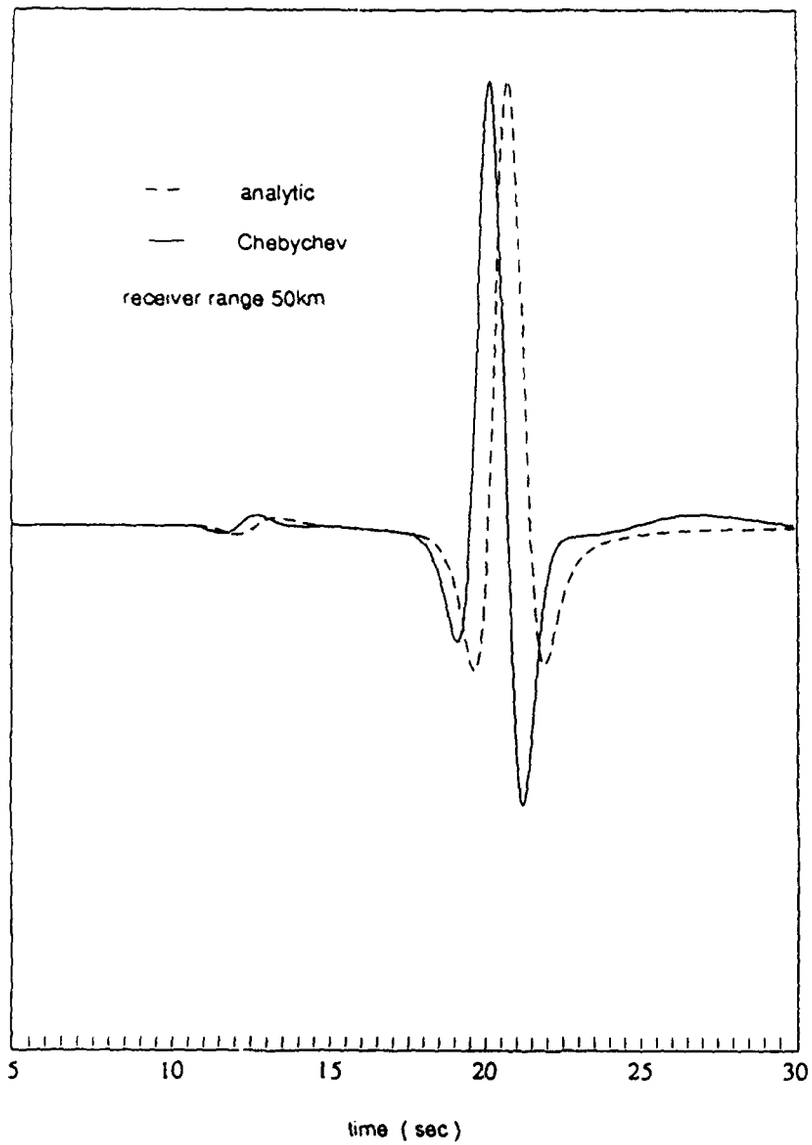

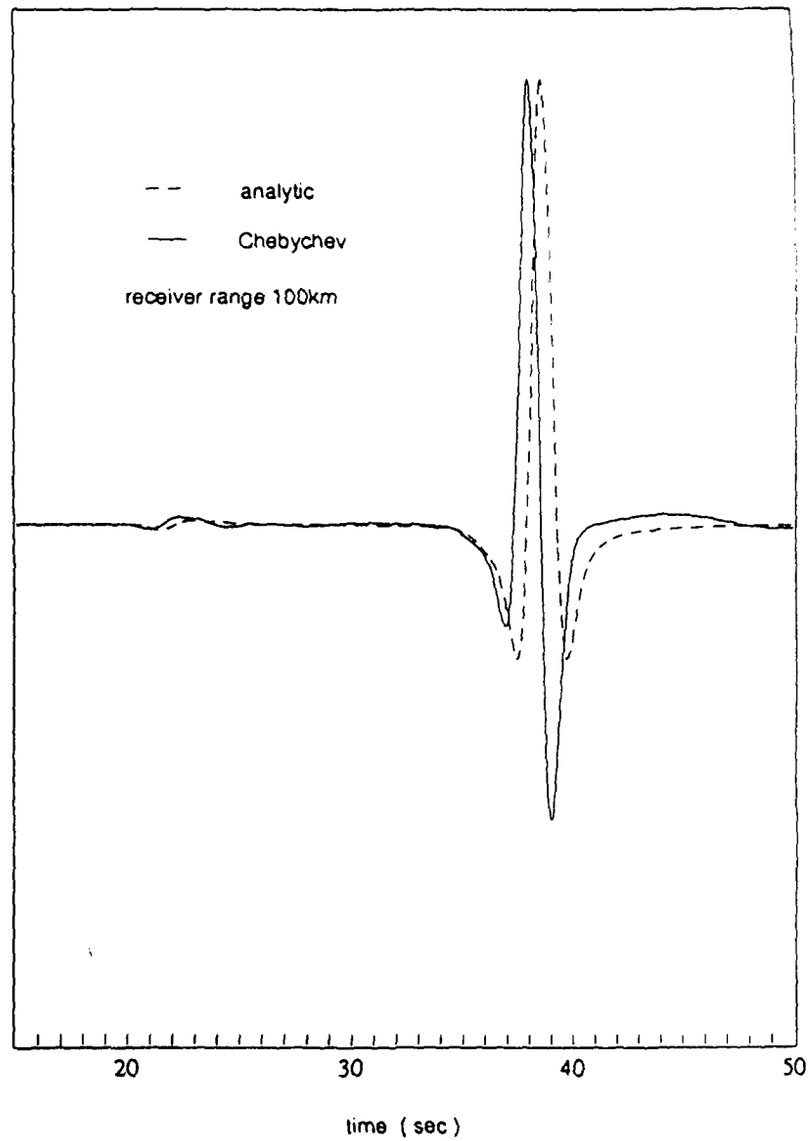

Figure 6-a: Lamb's Problem: Comparison of analytic and Chebychev solutions.

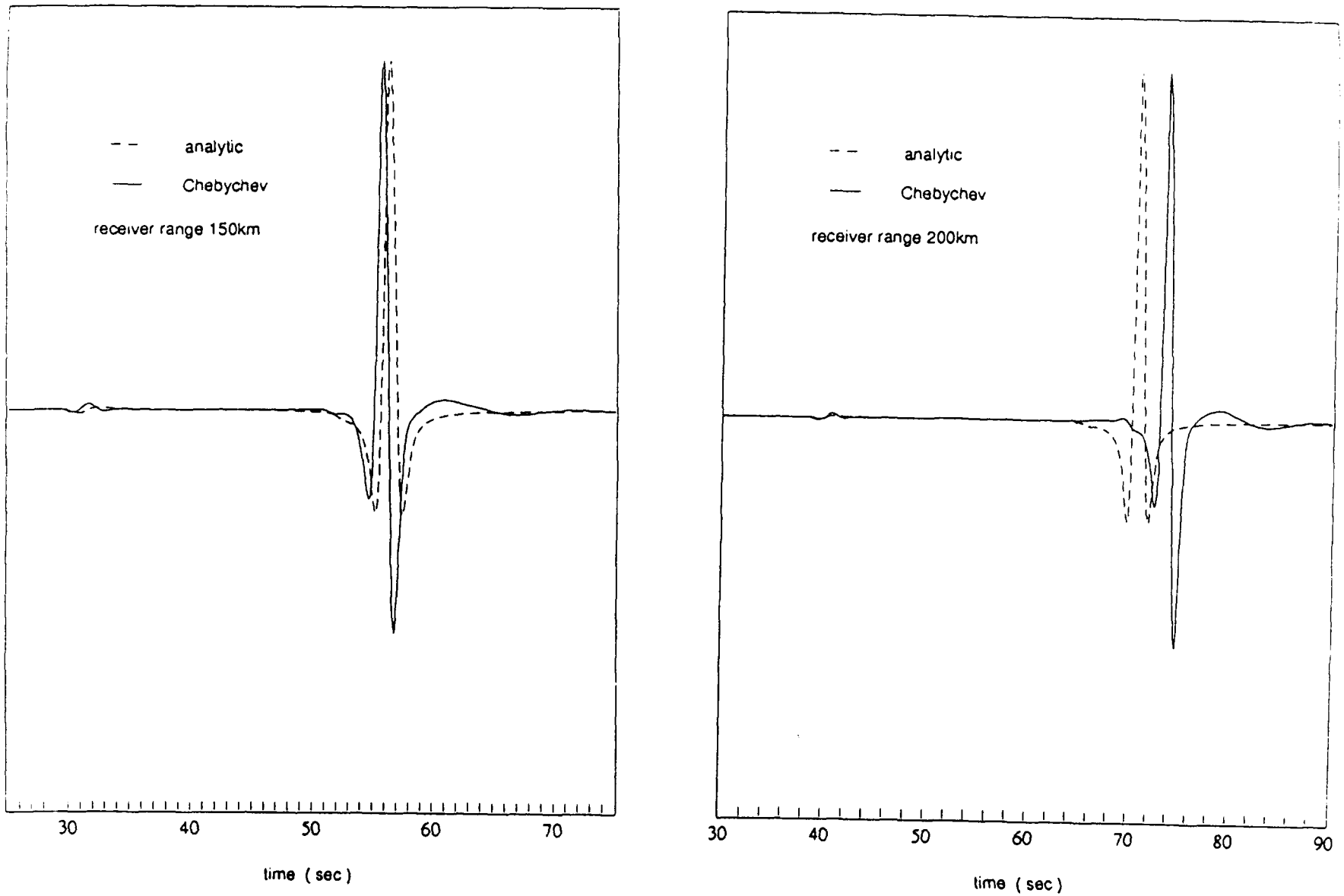

Figure 6-b: Lamb's Problem: Comparison of analytic and Chebychev solutions.

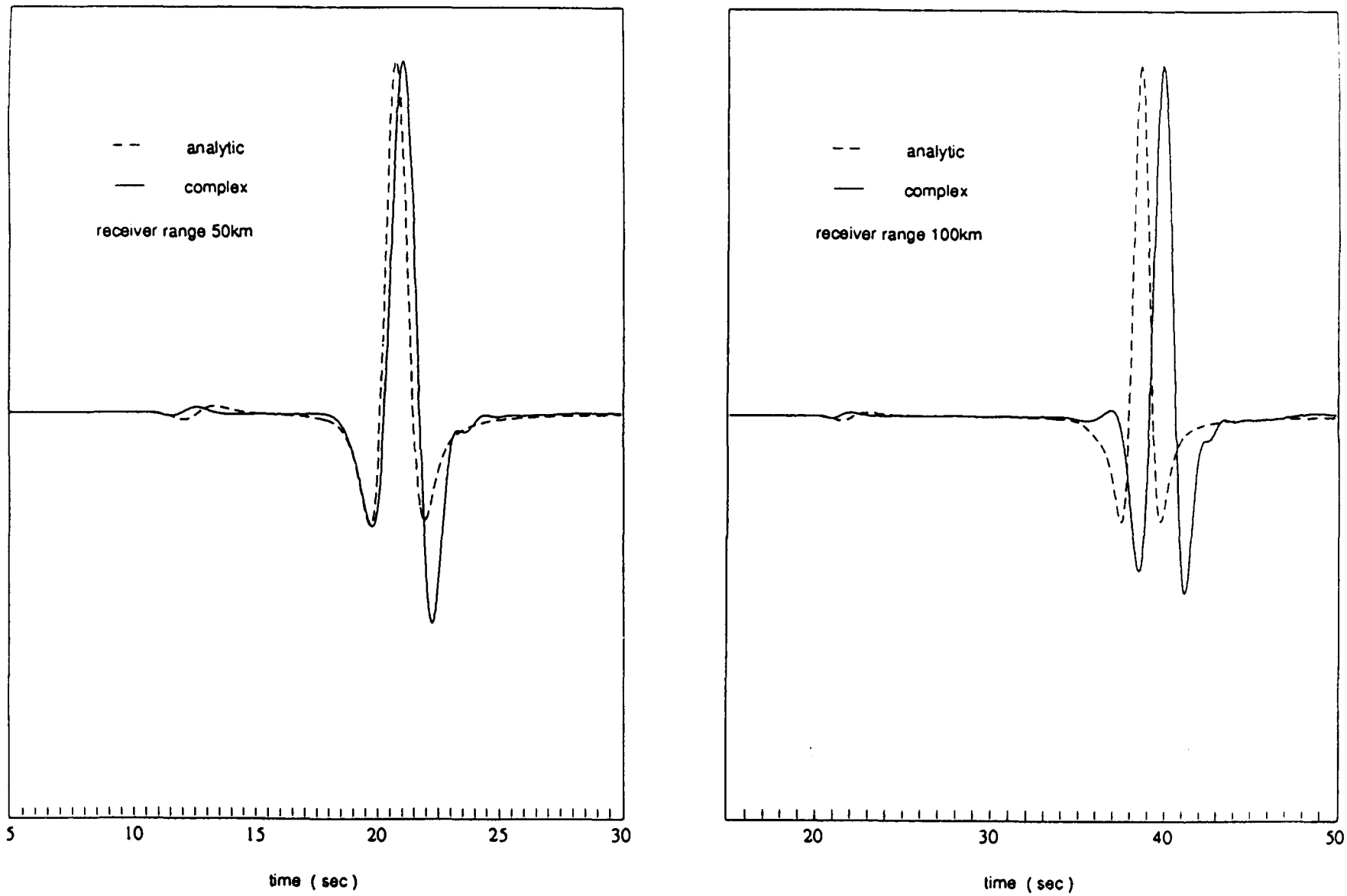

Figure 7-a: Lamb's Problem: Comparison of analytic and complex pseudospectral solutions.

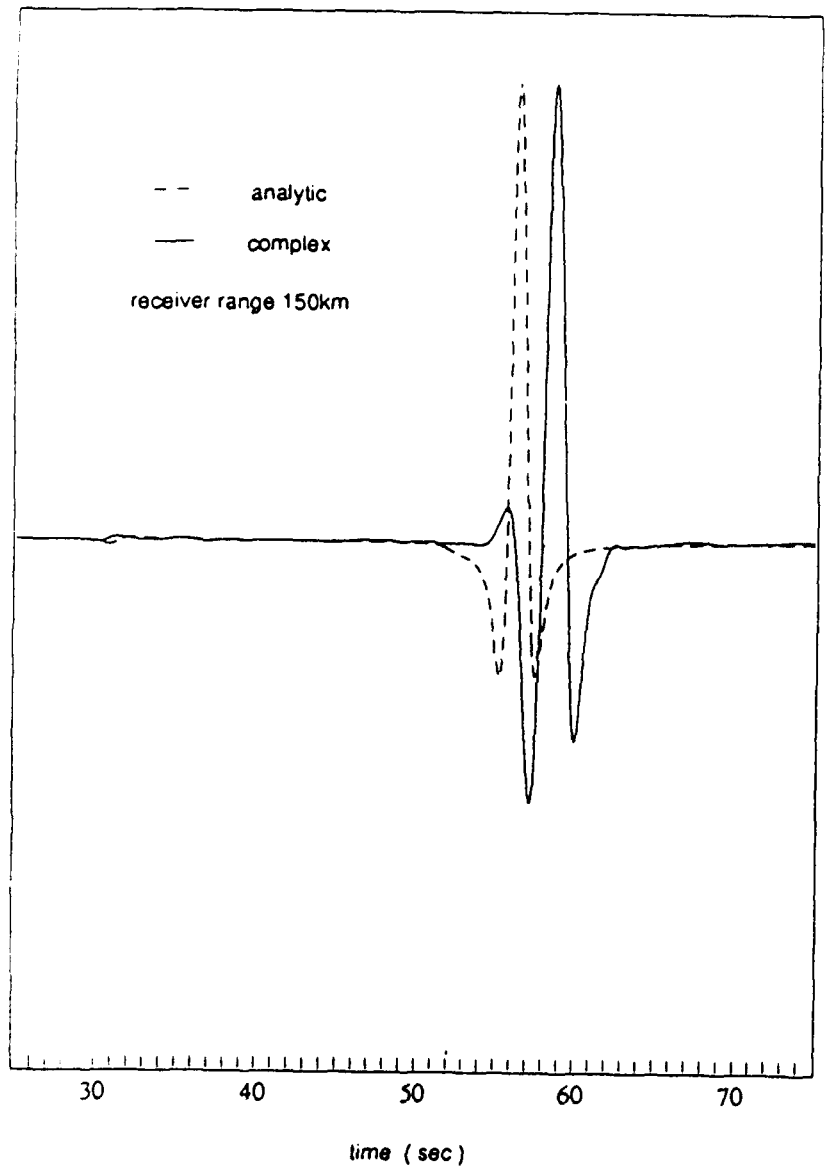

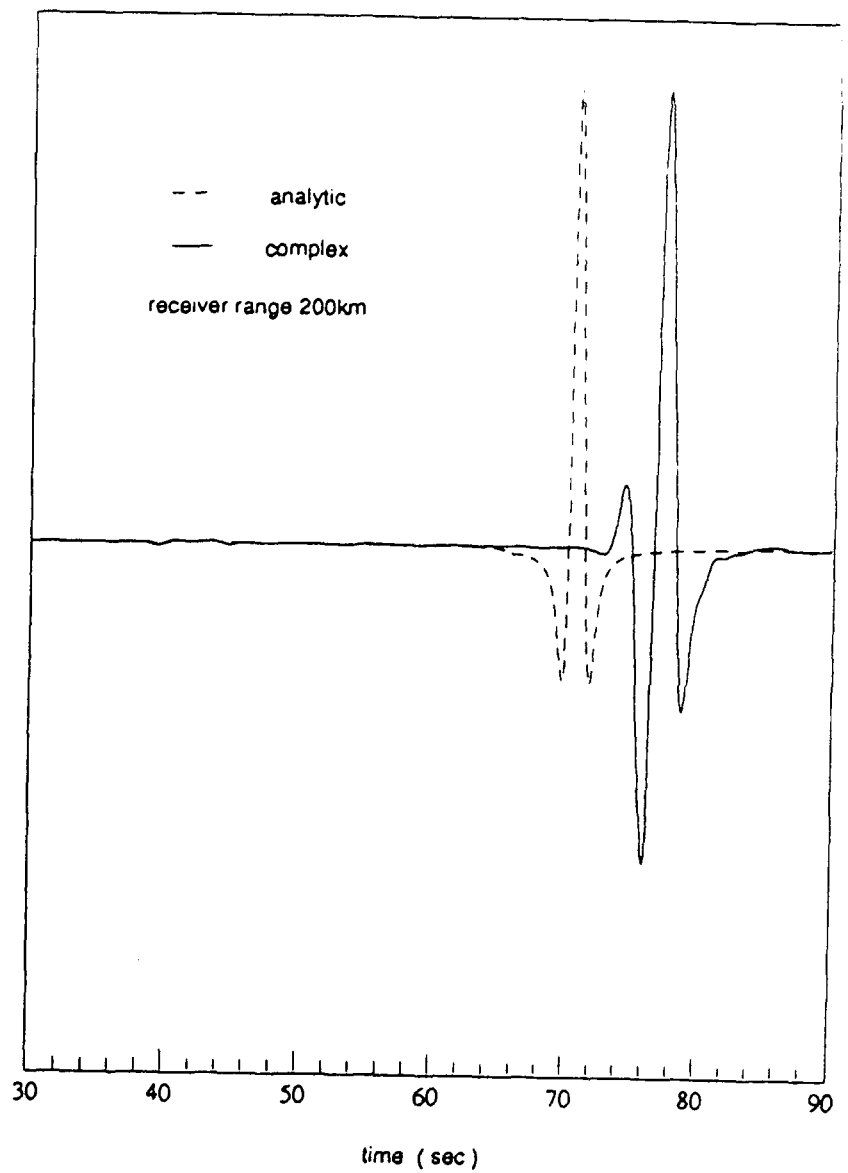

Figure 7-b: Lamb's Problem: Comparison of analytic and complex pseudospectral solutions.

for the solution in Figure 6. The grid spacing was chosen to give only 3 nodes per wavelength of the Rayleigh wave. The characteristics of the complex Fourier pseudospectral solution are different than those of the Chebychev solution, but it appears to be qualitatively of similar accuracy. However, there is a somewhat larger error in the Rayleigh wave arrival time (which increases with increasing distance) than for the Chebychev approximation.

The complex formulation requires doubling the storage for the velocity and stress variables, but the rapid use of complex FFT's can be retained without additional computational effort. In contrast to the Chebychev method, standard second-order accurate time integration is possible with the complex Fourier method. This allows larger time steps and a much simpler and therefore rapid time integration scheme.

Tests of the complex pseudospectral (CPS) method can also be made relative to 1D modal solutions (eg. Harvey, 1981). Here we expect the numerical CPS result to be quite accurate for body waves but that it may produce some error in the fundamental mode surface wave due to the abrupt velocity change represented by the free surface. The Modal theory will of course produce a very accurate representation of the low order surface wave modes so that this comparison, in a representative layer model of the earth's crust and upper mantle, should give us a good check on the accuracy of the CPS method for "realistic" models.

Figure (8) shows a Modal - CPS comparison for a layered earth model representative of the structure in the nuclear test site area in Kazakhstan. The agreement between the two computations for the surface wave is close, and the remainder of the seismogram is also in good agreement. We therefore consider the CPS method to be a

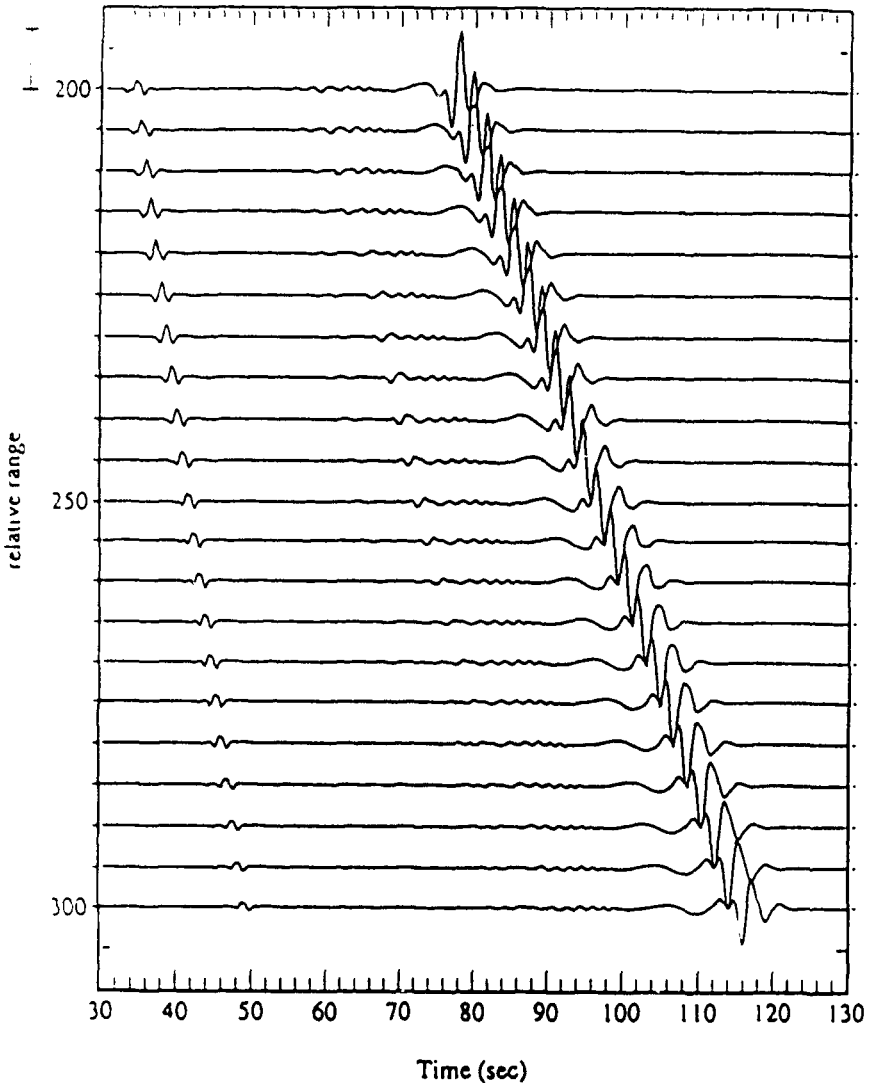

Figure 8-a: Complex pseudospectral synthetic seismograms for a layered earth structure. The explosion source was applied at a depth of 1km. with a maximum frequency content of 1Hz.

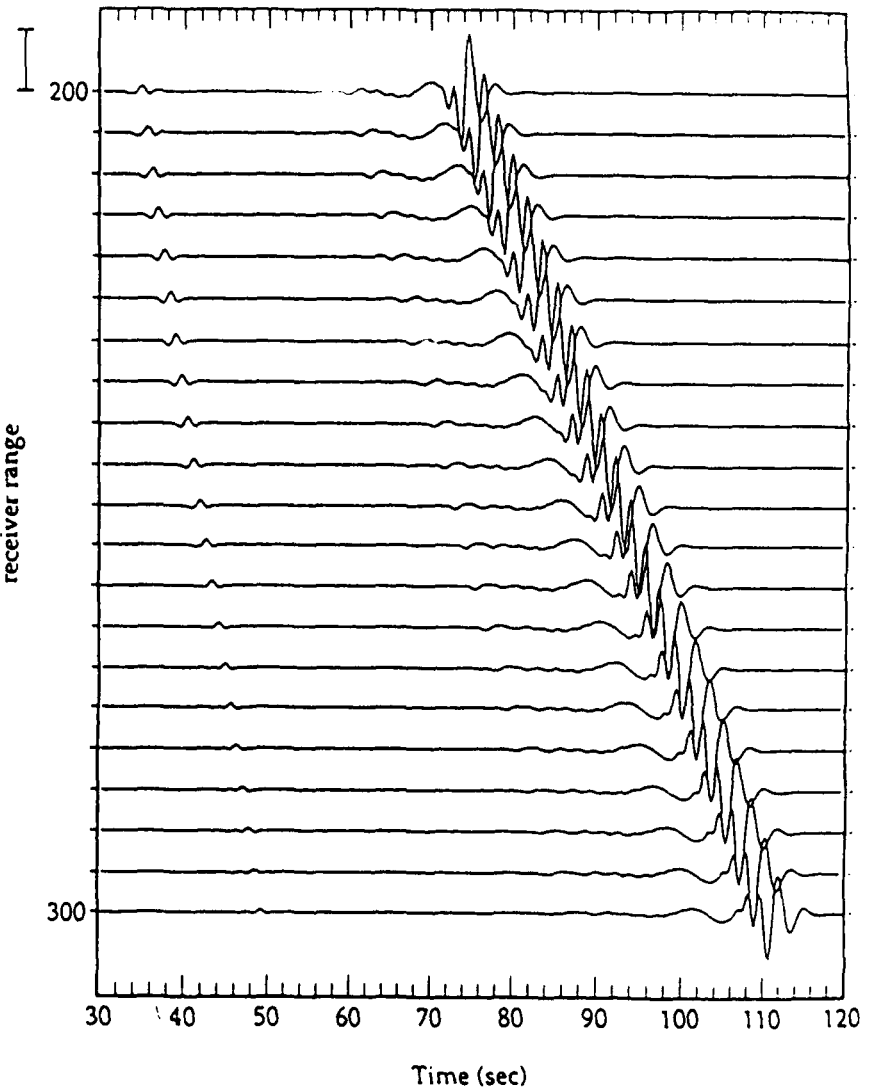

Figure 8-b: Normal mode synthetic seismograms for a layered earth structure similar to that used for Figure 8a. The maximum frequency content is 1Hz.

good and quite reliable means of computing seismic synthetics in complicated media. Nevertheless, we expect to be able to improve on it and eliminate the (relatively small) group delay errors by one of several modifications now under study.

Seismic Modeling Results for Complex Earth Models

At present 1D analytical methods, employing mode superposition methods, as described by Harvey (1981, 1991), are also being employed to compute synthetic seismic time series from a variety of source types. These are being compared to numerical modeling results as a check and, more importantly, to observed data. Here our objective is to systematically vary 1 D structures in a manner designed to test the limits of 1D modeling of regional seismic data. In this endeavor we are using "vertical randomization" of the structure (that is, superimposed random fluctuations on a mean velocity model that fits travel time data) to try to fit near field and regional observations from relatively simple explosion sources.

Figure (9), is an example of such comparisons. It is evident that by the use of superposed vertical randomization one can obtain reasonable first order fits to the data over at least the 0 to 1Hz frequency band. However, this is only the case in the regional distance range out to 200-300 km, at least near the Soviet East Kazakh test site, and only over the lower frequency range up to a few Hertz. In particular, it has become apparent that lateral variations become much more important when such simple 1D model results are systematically compared to more distant observations and/or compared to higher frequency data. It appears, at least in the southwestern Soviet Union, that lateral variations produce marked effects on the signal beyond distances corresponding to about fifty wavelengths in propagation distance. (This of course

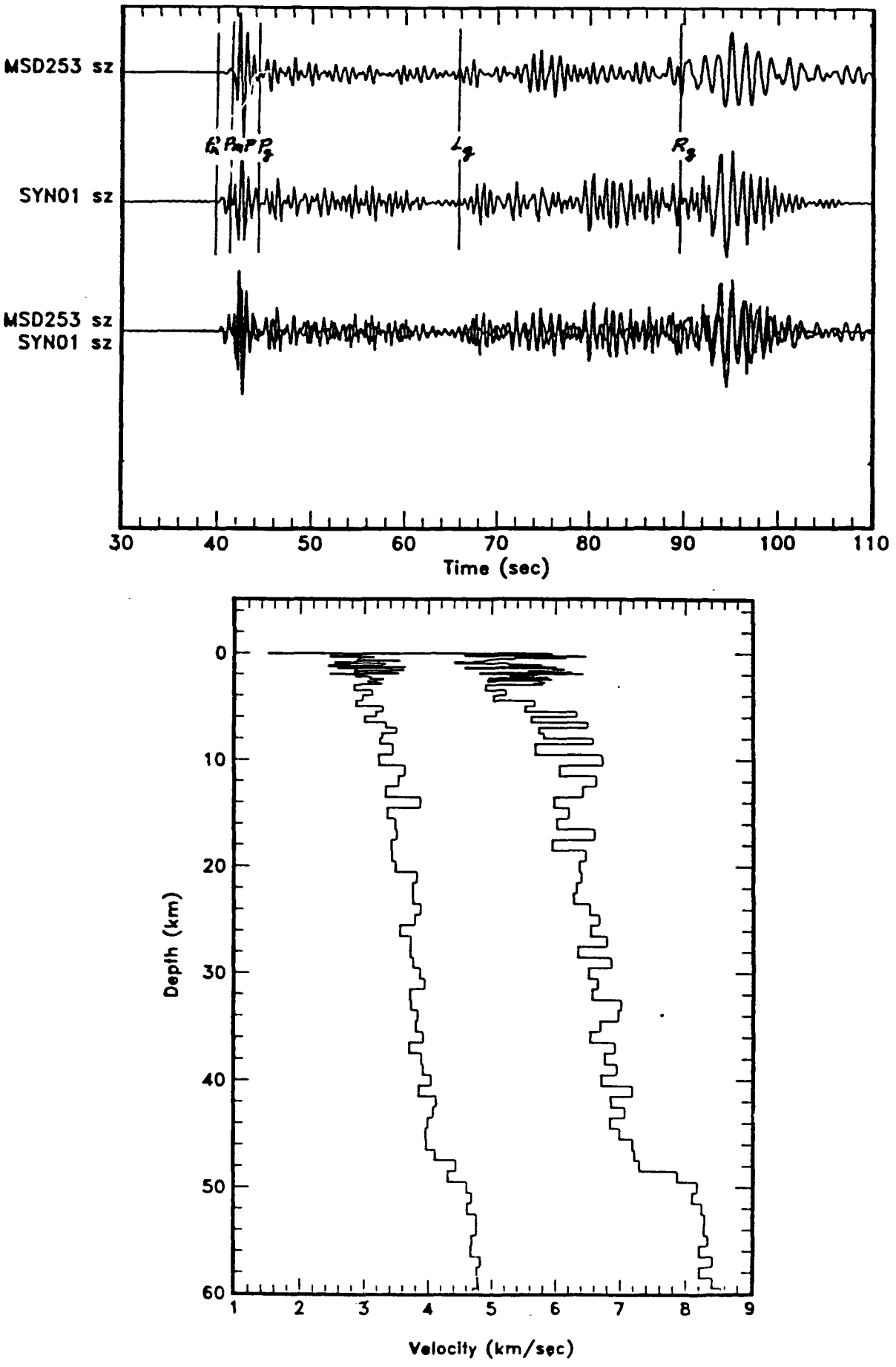

Figure (9.) Comparison of observed (MSD) and synthetic (SYN) seismograms for the Soviet Joint Verification Explosion (JVE) at 253 km. from the test. The velocity structure used to generate the synthetic is shown in the lower insct.

varies with wave type, with the P_g, L_g and R_g signals understandably showing the greatest sensitivity to lateral variations.)

Currently we are developing modal synthesis methods for 2 and 3D structures (Archambeau, AFGL annual report, 1990) employing lateral propagator methods. These will complement the purely numerical modeling methods described earlier and can result in marked advantages in computational speed and flexibility and may, it is hoped, be particularly useful in inversion procedures.

Both the numerical and analytic (modal) methods can be used to evaluate the effects of simple random spatial fluctuations in material properties in and vertical and horizontal directions within a layered earth model. Such computations would be a first step in assessing the importance of medium fluctuations and larger scale material property variability in the production of seismic wave fields seen in the regional distance range. Other more extreme and complex models can also be explored, but a logical first step it to investigate simple random variability from layered mean velocity models of the earth.

In this regard, we note that Figure (9) compares observed data and a synthetic seismogram generated from a 1-D vertically randomized mean velocity model. The mean velocity model was constrained to fit the travel time data obtained from studies in the region while the randomization used corresponds to fluctuations in seismic velocities and densities about there mean values, of about 15% near the surface to a few percent at depths in the upper mantle just below the crust-mantle boundary.

The fit of the synthetic to this single observed seismogram, recorded at a distance of 253 km. from the JVE nuclear test, is certainly not exact but has a structure that is

quite similar to that observed. The lower trace is an overlay of the synthetic on the observed time series. The velocity structure used is shown in the lower inset.

As noted earlier however, test computations at greater distances, using the same or similar velocity structures, does not produce good fits to observed data from this same event. In particular, the R_g wave is observed to attenuate very rapidly with increased distance and the R_g predictions do not attenuate nearly so rapidly and the observed P_g and L_g are larger than those predicted. We conclude from this that simple vertical randomization in the velocity structure is not sufficient to explain the basic first order properties of the data observed.

The next step is therefore to include a form of lateral variability in the earth models. The simplest variation that can be expected is lateral fluctuations in the medium velocities as well as the vertical fluctuations. Examples of the evaluation of models of this type are shown in Figures (10), (11) and (12). These results were generated using the CPS numerical method.

The various model fluctuations indicated in these figures are extreme enough to produce a range of results that allow an assessment of the role of material property fluctuations on seismic signal data; particularly the magnitude of the scattering effects on R_g , L_g , and P_g.

These results indicate that the likely spatial fluctuations in seismic velocities within the earth are not sufficient, by themselves, to explain the extreme attenuation of R_g with distance nor the large magnitude of the L_g and P_g wave trains.

It is therefore likely that large scale variations in shallow structure, coupled with material property fluctuations and anelastic attenuation are in combination responsible

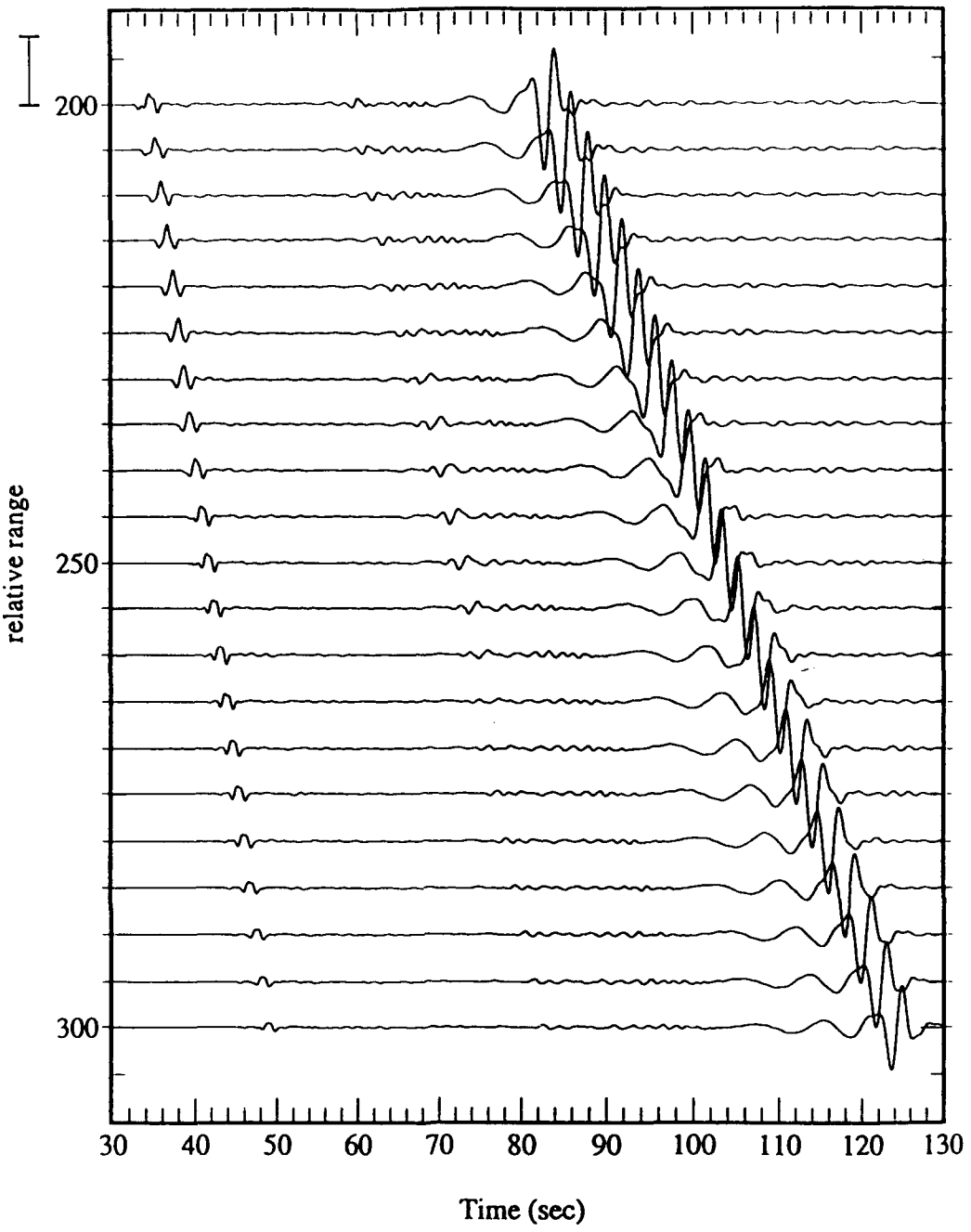

Figure 10-a: Synthetic seismograms for a layered earth with horizontal and vertical randomization of 1km. square segments of the earth structure. The fluctuations very smoothly from 20% at the surface to 3% at a depth of 3km.

Figure 10-b: Cross-sectional representation of the randomization applied to the layered structure.

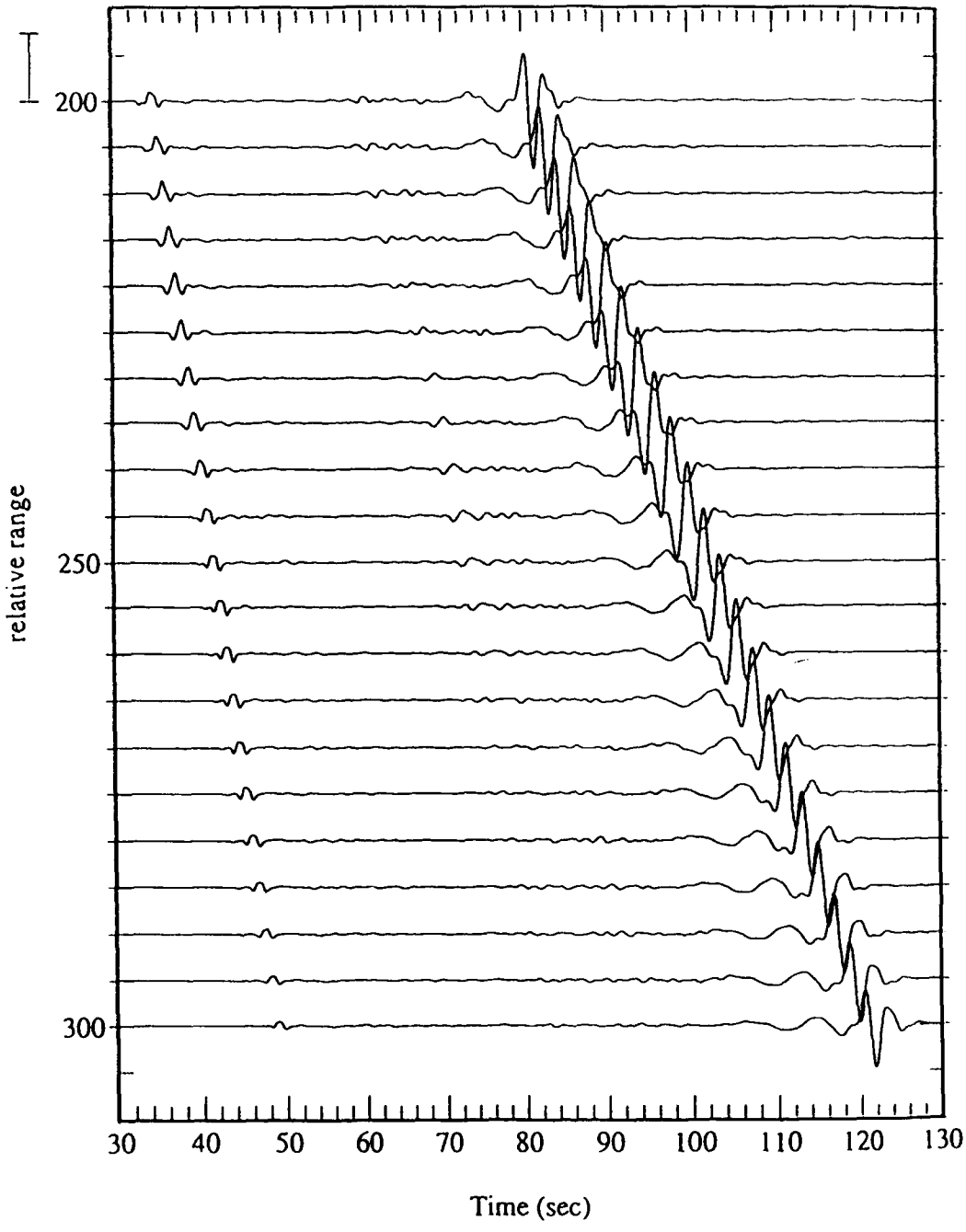

Figure 11-a: Synthetic seismograms for a layered earth with horizontal randomization of 4km-wide segments of the earth structure. The fluctuations vary smoothly from 15% at the surface to 3% at a depth of 3km.

Figure 11-b: Cross-sectional representation of the randomization applied to the layered structure.

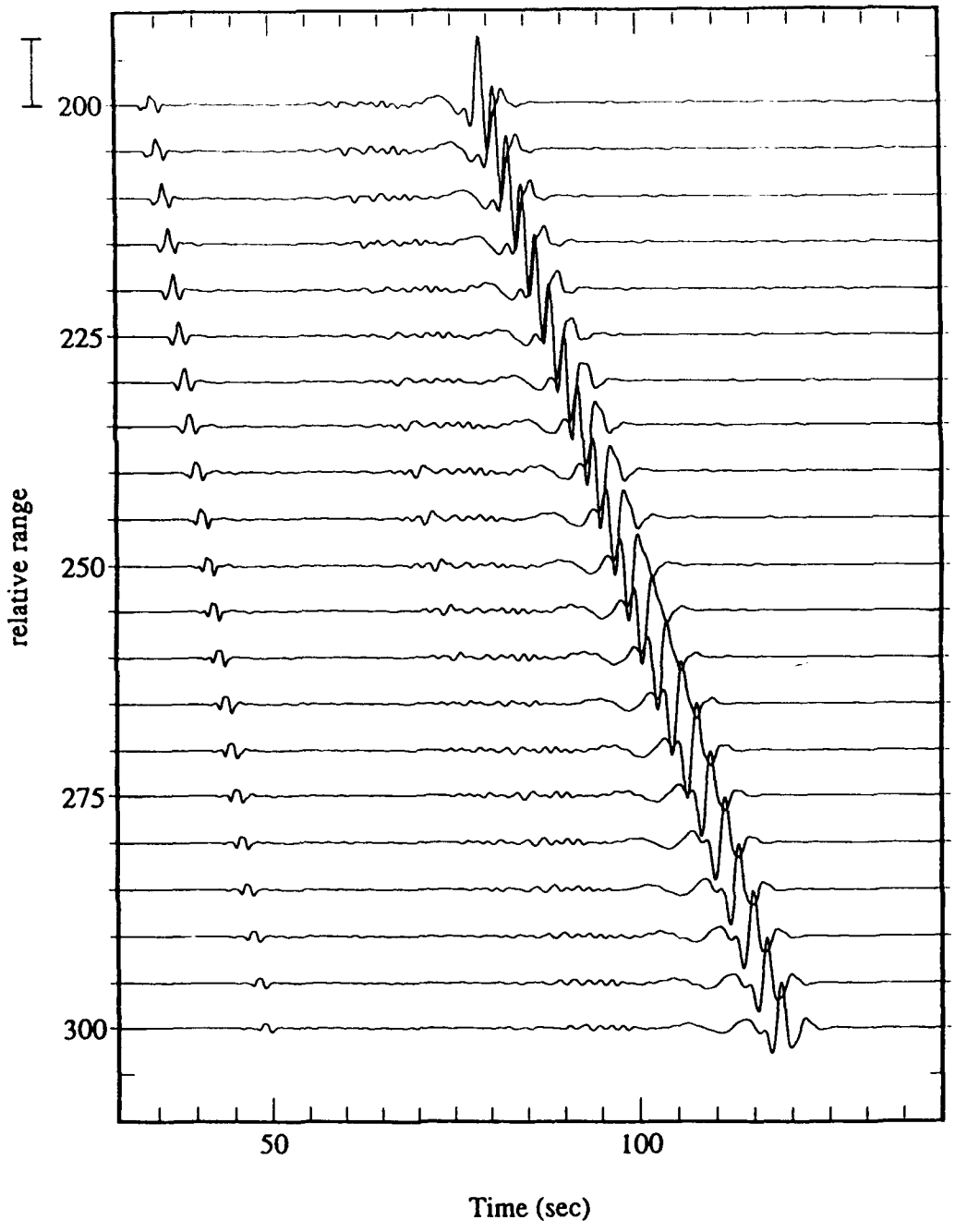

Figure 12-a: Synthetic seismograms for a layered earth with 12km-wide horizontally and vertically randomized segments placed every 36km. The fluctuations vary smoothly from 15% at the surface to 3% at a depth of 3km.

Figure 12-b: Cross-sectional representation of the randomization applied to the layered structure.

for the effects observed in the propagation of the major regional signal groups. The dominent effect for R_g and L_g is most likely to be strong large scale lateral variations. Future modeling studies will involve systematic investigations of these structure effects on the seismic data and we fully expect to be able to isolate the factors of importance given our current modeling capabilities.

As another example of the application of the seismic modeling, Figure (13) shows seismic time series computations that are designed to evaluate the effects of rough surface topography near a buried explosion source. The effects of shallow fine scale layering are also indicated by these examples. Clearly the examples show that complexities in the P and P_n coda of the type observed in the earth can be produced by topographic features and/or near source fine scale layering. In subsequent applications a generalized version of the current computer program will include non-linear effects, including failure, so that the effects of spallation (separation of near surface layers under explosive shock loading) can also be included. The effects of strong or moderate lateral variations in near source shallow structures can, of course, also be included now and may be systematically studied. Through this approach we plan to "sort out" the quantitative nature of each of these effects on the directly radiated seismic field from explosions and be able to evaluate their total impact on source depth estimates, yield estimation and discrimination.

In addition to near source effects modeling, we are using both analytical and new numerical methods to extend our computational range to greater regional and teleseismic distances. Most of these methods involve 2 and 3D modeling in order to be able to account for lateral variability in the medium. Currently restrictions imposed by

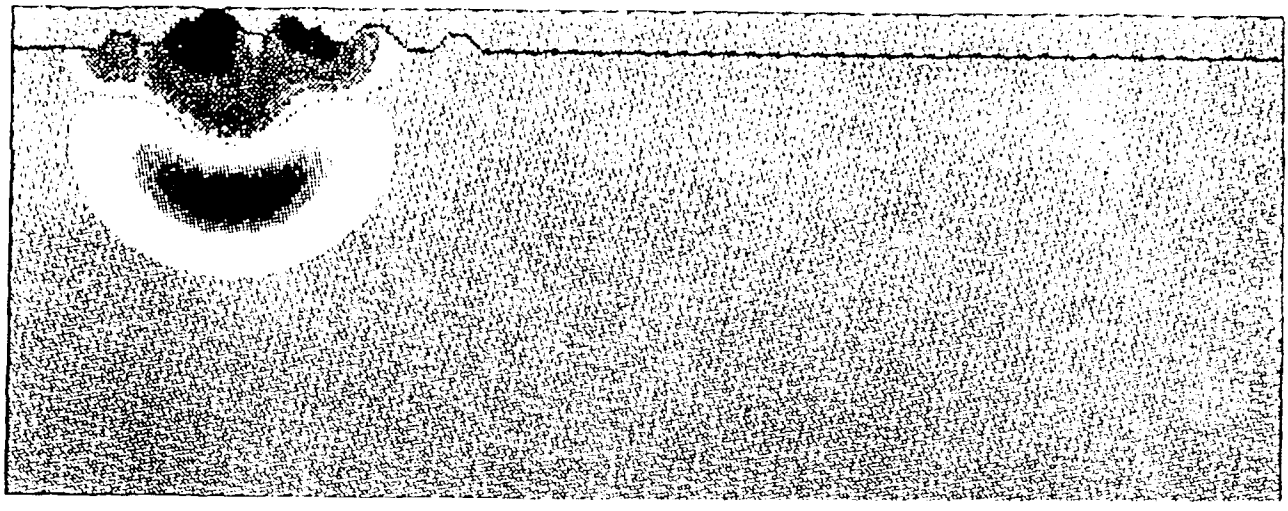

(a) Vertical Velocity Field, .32 sec after detonation

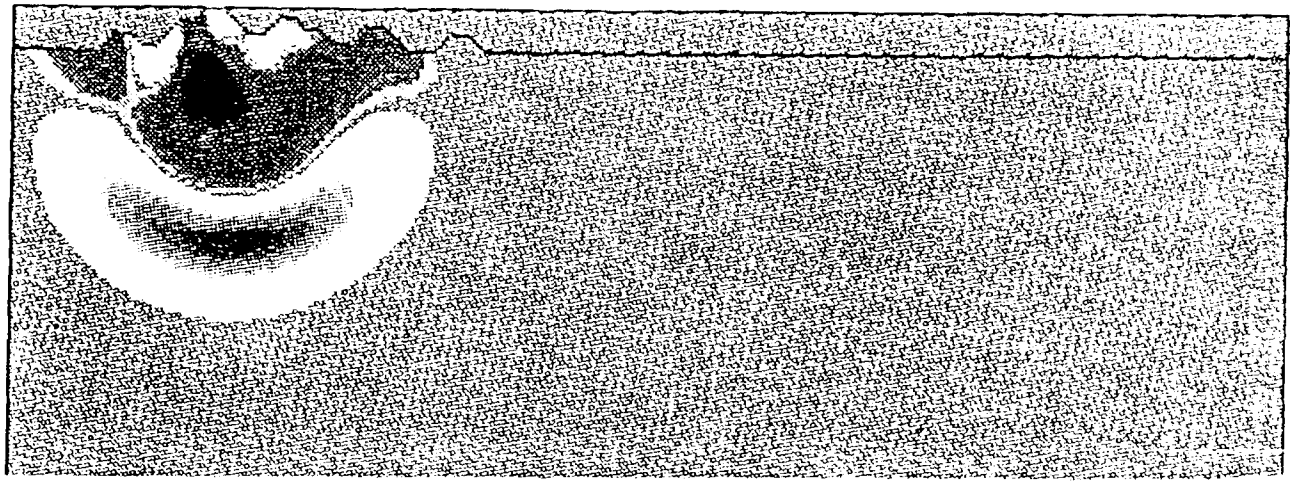

(b) Vertical Velocity Field, .38 sec after detonation

( ) Vertical Velocity Field, .58 sec after detonation

Figure (13-a.) Contours of the vertical particle velocity from an explosion 300 meters below the free surface with high relief surface topography in the vicinity of the source area. The dimensions of the cross-section shown is 9 km. wide by 3.45 km deep. Maximum surface elevation is 300 meters.

(a) Vertical Velocity Field, .71 sec. after detonation

(b) Vertical Velocity Field, .92 sec. after detonation

(c) Vertical Velocity Field, 1.15 secs after detonation

Figure 3 (a-c) Contours of the vertical particle velocity from an explosion 300 meters below the free surface with high relief surface topography in the vicinity of the source area. The dimensions of the cross-section shown is 9 km. wide by 3.45 km. deep. Maximum surface elevation is 300 meters.

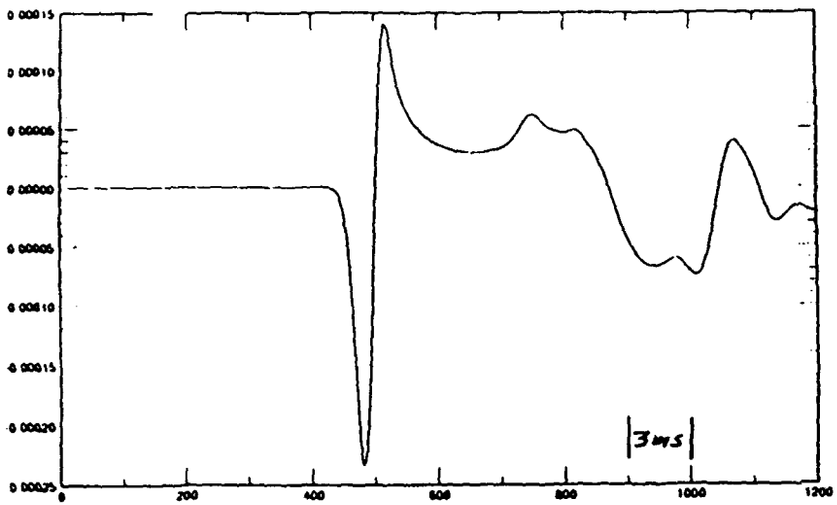

(a.) Vertical Velocity time series near the surface of an elastic *homogeneous* half space *without* surface topography.

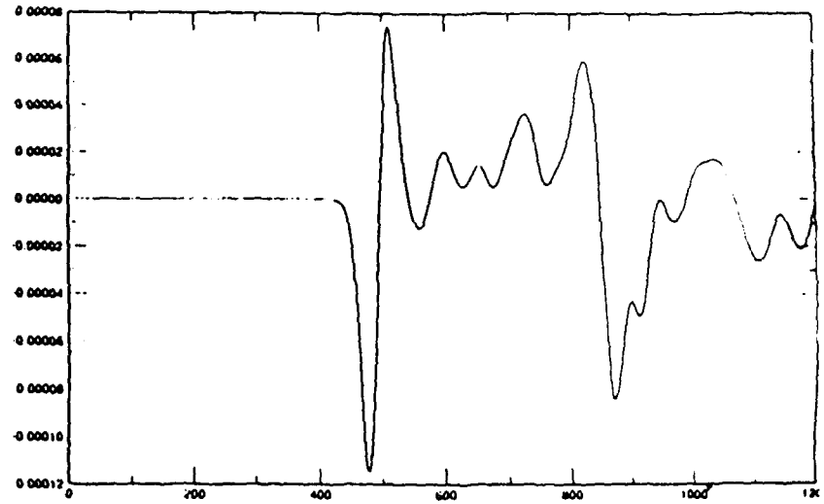

(b.) Vertical Velocity time series near the surface of an elastic *homogeneous* half space *with* rough surface topography near the source area.

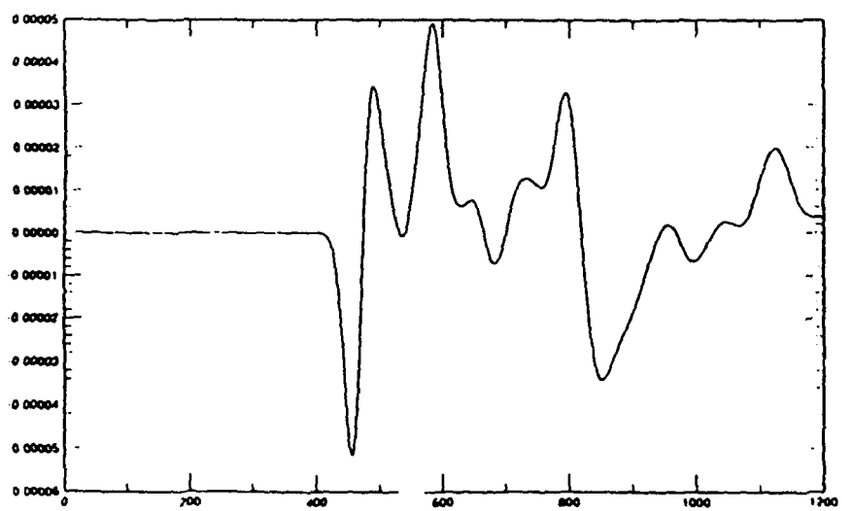

(c.) Vertical Velocity time series near the surface of a (5) *layered* half space *without* surface topography.

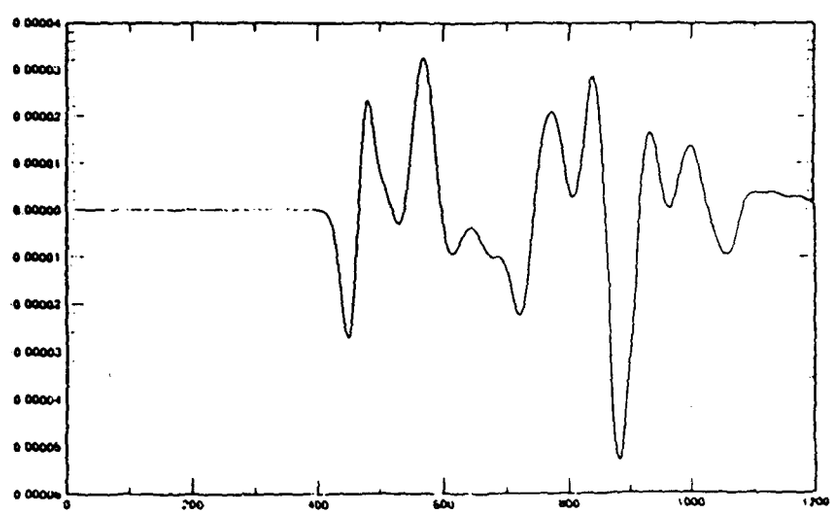

(d.) Vertical Velocity time series near the surface of a (5) *layered* half space with rough surface topography near the source area.

Figure (13-c.) The effects of near source topography and fine scale layering on the wave field from a buried explosion source (300 m. depth). Observations are at 6 km. from the source on the free surface.

computer memory and speed limitations confine the numerical seismic modeling applications, in 2D, to distances of less than 1000 km and to frequencies less than 1-2 Hz. Modeling in 2D to frequencies of 20-30 Hz is usually limited to distances of about 100 km from the source. By developing moving grid methods and FFT evaluations of partial derivatives, which have already been tested, we expect to be able to model high frequency wave fields throughout the regional distance range to a few thousand kilometers and the primary teleseismic signals (body waves) to all distances.

IV. Modeling Atmospheric Wave Fields and Ionospheric Electron Density Variations Due to Near Surface Seismic Sources

Because of the exponential decrease of atmospheric density with height, buoyant pulsed gravity waves generated by surface or subsurface seismic sources can be of appreciable amplitude throughout the atmosphere. Furthermore, above 100km in height, these flow transients affect the ionospheric E-M fields through changes in the distribution of the charged particles. The basic equations governing motions of the neutral atmosphere are the conservation laws of mass, momentum and energy together with the ideal gas equation of state. The specific nonlinear continuum equations incorporate nonlinear advective terms as well as the gravitational field, gas compressibility, viscosity effects and thermal conductivity. For electron motions in the ionosphere a first-order continuity equation can be used as a first approximation which assumes that electrons move with the neutral atmosphere.

For modeling purposes, the set of partial differential equations for the atmosphere are converted to a corresponding set of finite difference equations in order to effect numerical integration in time and space. The non-linear terms are treated non-locally

on the lattice for stability, effectively controlling, internally, the instabilities. In addition, random velocities and pressures are attributed to the inherent fine scale turbulence in the atmosphere and are incorporated in the modeling, as are mean drift particle velocities. In particular, in order to account for the inherent turbulence in the atmosphere, the flow variables at a point are decomposed into a mean flow, governing winds and a perturbed flow that incorporates the turbulence. A new approach, designed to include turbulence, has been developed using random perturbations, obtained from a random number generator, which are inserted directly into the finite difference equations. Turbulence is also produced by a random distribution of temperature at the surface which produce thermal structures with upward and downward flows. Horizontal winds, impacting on a variable and random topography, also produce upward and downward motions which have a random stochastic character.

The set of non-linear partial differential equations are converted to a corresponding set of finite difference equations for numerical integration in time and space and upwind differencing is used for first order spatial gradients with the advection velocity terms acting at the upwind point. However, if the velocity operates on its own velocity gradient, such non-linear terms are treated non-locally on the lattice for stability, effectively controlling internally any unstable growth.

There are at least three types of boundary important to the modeling of fluid flows. Specifically, the air-ground surface is topographically complex with a turbulent boundary layer of the order of a few meters at the interface. At this boundary, vertical velocities are random both in time and spatial locations. Because of the presence of the lower boundary layer above a complex topography, horizontal velocities are not

taken as zero but incorporate winds and turbulence effects. The top atmospheric boundary is open, with decreasing density. The topmost boundary should mimic the conditions for an open atmosphere with specific considerations for buoyancy and field gradients. We have examined various options including fixing velocities and densities and their gradients. However, we have adopted the general open flow boundary, which we also use for the artificial side boundaries. The side boundaries are artificial, due to grid restrictions, and must mimic open boundaries that allow free flow in either direction. We have adopted the more usual approach, wherein the dependent variables are constrained to stay constant at these open boundaries.

Explosive sources at and below the ground are simulated by stress distributions and velocities along the earth's surface and their resultant effects on the atmosphere are integrated upward and outward. Various velocity sources are used at the lower boundary with differing time, amplitude and radial dependences. The standard input is a source, comprised of the first differential of a gaussian in time, that approximates the initial pulse from an underground explosion. Cartesian coordinates are used to model the 3-dimensional system, with the source at the center of the bottom plane.

Conservation Laws

The continuity equations are based on the values of the fields at particular points in space and time. Conservation of mass is expressed as,

$$\frac{\partial \rho}{\partial t} + \frac{\partial}{\partial x_j}(\rho u_j) = 0 \qquad (1.)$$

where ρ is density and u_j is velocity in the x_j direction. Conservation of momentum is similarly expressed as:

$$\rho\left[\frac{\partial u_i}{\partial t} + u_j \cdot \frac{\partial u_i}{\partial x_j}\right] = \rho X_i + \frac{\partial}{\partial x_j} \cdot P_{ij} \qquad (2.)$$

where X_i are external forces, P_{ij} is the generalized stress such that:

$$P_{ij} = -p\cdot\delta_{ij} + 2\mu\cdot e_{ij} - 2/3\mu\cdot\delta_{ij}\cdot e_{kk} \qquad (3.)$$

with $e_{ij} = 1/2\left[\frac{\partial u_i}{\partial x_j} + \frac{\partial u_j}{\partial x_i}\right]$ the strain rate and μ the viscosity. Conservation of energy is:

$$\rho\cdot\frac{\partial}{\partial t}(c_v\cdot T) + \rho u_j\cdot\frac{\partial}{\partial x_j}(c_v T) = \frac{\partial}{\partial x_j}(K\cdot\frac{\partial T}{\partial x_j}) - p\cdot\frac{\partial u_j}{\partial x_j} + \Phi \qquad (4.)$$

where T is temperature, c_v is specific heat at constant volume, K is thermal conductivity, and Φ is the viscous dissipation. Here:

$$\Phi = 2\mu e_{ij}^2 - 2/3\cdot\mu(e_{jj})^2$$

The equation of state for the atmospheric gas is taken to be ideal, i.e.

$$P = \frac{k_B}{m}\cdot\rho\cdot T \qquad (5.)$$

where k_B is Boltzmann's constant and m is the mean molecular weight.

Normalized Equations

In the fundamental equations, (1) through (5), the dependent and independent variables can be normalized with respect to typical values. For an ambient atmosphere, with exponential decay of density with height, distances are normalized through the scale height, H, which, at the surface, is approximately 8400 metres. Velocities are normalized with respect to c_s, the sound velocity of air at the earth's surface. Similarly density, pressure and temperature are normalized to surface values, and the independent variable, time t, is normalized by (H/c_s). Thus for the continuity

of mass, we get, as before,

$$\frac{\partial \rho}{\partial t} + \frac{\partial}{\partial x_j}(\rho u_j) = 0 \qquad (6.)$$

where the new variables are now normalized and given the same symbol as the original variables. Incorporating gravity as the external force, the momentum conservation equation, (2), becomes

$$\rho \cdot \frac{\partial u_i}{\partial t} + \rho u_j \cdot \frac{\partial u_i}{\partial x_j} = -G_s \cdot g(z) \rho \cdot e_z - A_2 \cdot \frac{\partial P}{\partial x_i} + A_4 \cdot \Psi_i \qquad (7.)$$

where $G_s = (g_s H / c_s^2)$ is a measure of the ratio of potential energy to thermal energy.

$A_2 = p_s/(\rho_s c_s^2)$ is a measure of the ratio of stress energy to thermal energy.

$A_4 = \mu_s/(\rho_s \cdot c_s)$ is the ratio of viscous to thermal energy.

Ψ is the normalized viscosity drag force,

$$\Psi_i = \frac{\partial}{\partial x_j}\left\{ \mu \left[\frac{\partial u_i}{\partial x_j} + \frac{\partial u_j}{\partial x_i} \right] - 2/3 \cdot \mu \cdot \frac{\partial u_k}{\partial x_k} \cdot \delta_{ij} \right\}$$

where μ is normalized to μ_s, the viscosity at the surface. In the atmosphere, μ is usually taken to be constant for the molecular viscosity. In the case of conservation of energy, the normalized equation is

$$\frac{\partial T}{\partial t} + u_j \cdot \frac{\partial T}{\partial x_j} = A_8 \cdot \frac{\partial^2 T}{\partial x_j^2} - A_6 \cdot \frac{\partial u_j}{\partial x_j} + A_5 \Phi \qquad (8.)$$

where

$$A_5 = \mu_s \cdot \frac{k_b}{m \cdot c_v} \cdot \frac{c_s}{(p_s \cdot H)} = A_6 \cdot \frac{A_4}{A_2}$$

$$A_6 = \frac{k_b}{m \cdot c_v}$$

$$A_8 = A_6 \cdot K \cdot \frac{T_s}{(p_s \cdot c_s \cdot H)}$$

where K is, as usual, taken constant for the atmosphere. The equation of state, on normalization, is

$$p = \rho \cdot T \cdot / m(z) \tag{9.}$$

where the ideal equation of state at the surface is $p_s = \frac{k_B}{m_s}\rho_s T_s$ with m_s the surface value of mean molecular weight (29.0) and m(z) the height-dependent normalized value.

Ionospheric Motions

The basic conservation law of charged particles, assuming no creation or annihilation, is:

$$\frac{\partial N_\alpha}{\partial t} = -\frac{\partial (N_\alpha \cdot u_{j\alpha})}{\partial x_j} \tag{10.}$$

where N_α is the number of particles of type α and $u_{j\alpha}$ is their velocity in the j'th direction. The initial concentration of the charged particles is taken to be time-independent, with only a vertical functional dependence, N(z), where the subscript α has been dropped for the type of particle. Assuming only small changes in this concentration, the dependence can be found from integrating eqn. (10) over the range t_0 to the present. To zeroth order, this concentration change becomes:

$$\delta N(z,t) = -\frac{\partial N(z)}{\partial z} \cdot \int_{t_0}^{t} u_z(t')dt' - N(z) \cdot \int_{t_0}^{t} \frac{\partial u_j(t')}{\partial x_j} dt' \tag{11.}$$

The first term in (11) is the concentration change due to the displacement of the ionospheric layer, while the second term arises as a result of compression or rarefaction and is the predominant term when dealing with processes involving characteristic dimensions smaller than the width of the layer. The velocity of the charged particle is

usually assumed to be identical with that of the neutral gas to zeroth order and this is the velocity that is used in the finite difference calculations for electron density changes.

The initial concentration of electrons is taken to be that of a Chapman distribution which has a maximum density at 345 km height and decreases rapidly below about 90 km with the functional dependence on height defined by:

$$N(z) = N_c \cdot \exp(\tfrac{1}{2}(1-\xi-e^{-\xi})) \qquad (12.)$$

Where $\xi = (z-h_c)/H$, $h_c = 345$ km, $H = 65$ km and N_c is the normalizing value.

Finite Difference Scheme

The set of non-linear partial differential equations are converted to a corresponding set of finite difference equations for explicit computer integration in time and space. Upwind differencing is used for first order spatial gradients, with the advection velocity terms acting at the upwind point. However, if the velocity operates on its own velocity gradient, such non-linear terms are treated non-locally on the lattice for stability, effectively controlling internally any unstable velocity growth.

The updated variable is projected not from just the old dependent variable, a process that is inherently unstable, but from a distributed smoothed average of the variable at locations surrounding the specific spatial location. Such a smoothing method brings stability to the differencing scheme. However, the attendant numerical diffusion is minimized by not smoothing the density variable, which has only a small effect on stability. This approach also helps in stabilizing the integration at grid corners and boundaries. The second order derivatives in the viscosity and thermal conductivity

terms are modeled by finite differences taken at the surrounding spatial locations.

In the explicit integration scheme, the updated flow velocities, temperature and density are obtained via their continuity equations while pressure is obtained from insertion of the updated density and temperature into the ideal gas equation.

Boundary Conditions

There are at least three types of boundaries important to the modeling of fluid flows. The air-ground surface is topographically complex with a turbulent boundary layer attached. The top atmospheric boundary is open to space with decreasing density. The side boundaries are artificial, due to grid restrictions, and must mimic open boundaries that allow free flow in either direction.

At the bottom boundary vertical velocity functions are input as sources of momenta at spatial locations. Otherwise, as usual, vertical velocities are taken to be zero at the bottom. Because of the presence of the lower boundary layer above a complex topography, horizontal velocities are not taken as zero but, instead, constant velocity and density gradients are assumed in the vertical direciton. For subsurface sources only momentum inputs are considered at this bottom boundary. For sources at or above the surface, both momentum and pressure conditions must be applied, just as in atmospheric sources.

The top-most boundary should mimic the conditions for an open atmosphere with specific considerations for buoyancy and field gradients. We have examined various options including fixing velocities and densities and their gradients. However, we have adopted the general open flow boundary, much as we use for the artificial side boundaries. As usual, in order to preserve conservation relations, all normal gradients are

set to zero at these open boundaries. However, this would not permit heat flow through the boundary. Therefore the second-order normal derivative of temperature is made constant.

Turbulence Effects

In order to account for the inherent turbulence in the atmosphere below the thermopause, the flow variables at a point can be decomposed into a mean flow and a perturbed turbulent flow. In the momentum equation, additional components are thus obtained for the generalized stress. These are mainly interaction terms between the mean and perturbed densities and velocities, termed the Reynold's stresses, which represent the interaction of the mean flow with the background turbulence. These extra stresses have been approximated by various phenomenological approaches. Boussinesq introduced the concept of eddy viscosities in order to use the Newtonian equations with the usual but much larger viscosity term. Our models evaluate the efficacy of this method using an eddy thermal conductivity. We also attempt to evaluate different forms of these Reynold's stresses through algorithmic modeling of various drag forces that mimic the effect of these interaction terms. It is found that even small drag forces of a particular type can alter the flows and their temporal dependence. An alternative approach to turbulence is developed in the use of random perturbations, obtained from a random number generator, and input directly into the finite difference equations.

Modeling Results

The result of the atmospheric modeling for effects of a surface explosion can be summarized as follows:

(1.) A time dependent transient pulse propagates upward from the seismic wave perturbation of the ground surface and has increasing amplitude relative to the ambient pressure. This produces asymmetric flows which control the flow development and the upward propogation of the transient. The initial positive density pulse is propagated upward more slowly than the following negative density pulse which has increased buoyancy. This initiates a sequence of circulation patterns that develop through what appears to be asymmetric triangular modes across the horizontal cross-section. The circulation patterns for the phenomena are characterized by upward central motions of the lighter matter, which, at the neutral buoyancy level, push outward to the side. The centroid of the transient pulse initially moves upward rapidly, but slows down to the group velocity speed of sound in the atmosphere. The advected air mass tries to remain in its horizontal stratification in order to minimize changes in its gravitational potential. However, it appears that energy and momenta are transported through traveling waves in the circulation pattern. Similar effects have been observed in the real atmosphere when thermals propagate upward from the Earth's surface with similar circulation patterns.

(2.) After a model-dependent characteristic time a bifurcation of the flow occurs with the eventual reversal of the velocity direction. The bifurcation phenomena occurs, in this model, every 100 seconds, so that it has a period of just over 3 minutes. A drag force is input in order to model the effect of the inherent background turbulence of the atmosphere. Such a drag force, which removes 2% of the component velocities at each computational grid pount at each time step, removes the periodic bifurcation and a standing wave is formed in the atmosphere

with constant field patterns. However, with a 1% removal rate, the patterns are periodic with similar bifucations as in the zero drag case. Because existing atmospheric turbulence acts on the transient gravity wave as a perturbation, we have also modeled its effect by imposing a random component on each field at each time step and grid point. The usual bifurcations are obtained but with differing patterns from the zero turbulence case. However, the appearance of the pressure and density fields is more realistic due to added diffusion and random components.

As the transient pulse moves upward in the atmosphere, it magnifies in amplitude relative to the exponentially decreasing ambient pressure. Thus, the level at which a specific pressure is located will oscillate as the transient pressure pulse moves through.

To the first order, the electrons in the ionosphere are assumed to move with the flow of the dominant neutrals. Thus the change in the electron density can be calculated from a conservation law, whose integration in time gives the total electron density variation. The ambient electron density is approximated by the Chapman function which has a maximum electron density at 350km and effectively zero electron density below about 90 km. For reasonable synthetic velocity sources at the ground surface, we find that changes in electron density from 100km and up are of the same order as those observed in E-M experiments conducted for surface and subsurface explosions.

In this regard, Figure (14) shows an example of the predicted fluctuations in temperature and electron density in the ionosphere due to a near surface underground explosion. In this case the explosion was taken to be a tamped underground nuclear test at a depth of 300 meters with a seismic body wave magnitude near 5. (Much

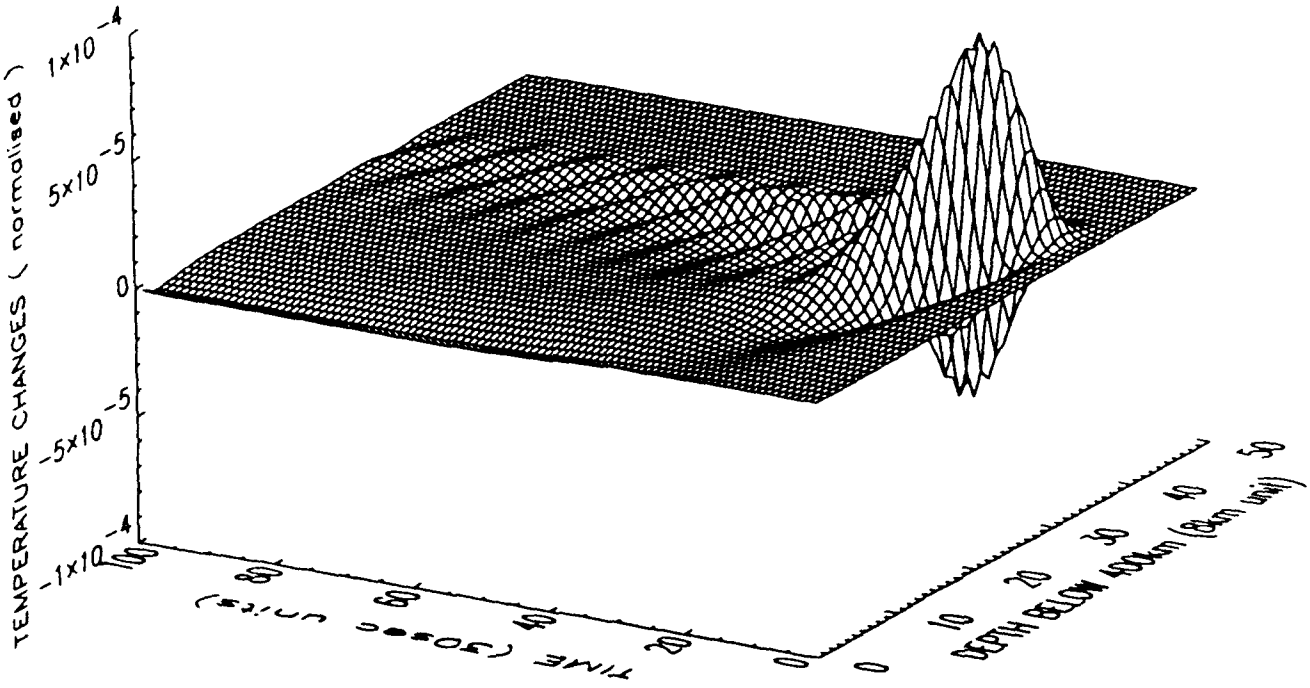

(a.) Time and spatial variation of the temperature change expressed as a fractional change in the temperature.

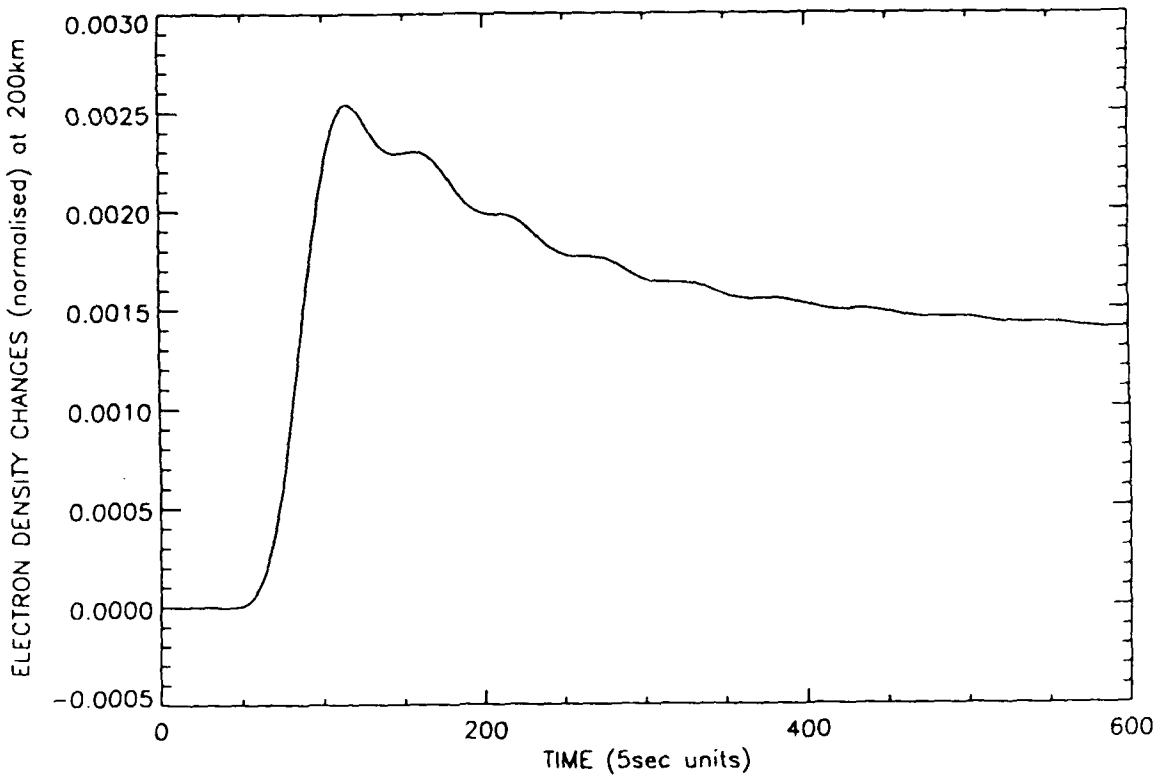

(b.) Time variation of the electron density change expressed as a fractional change in the electron density at 200 km. altitude.

Figure (14.) Fluctuations in the ionospheric temperature and electron density due to a transient pressure pulse at the earth's surface from a near surface explosion.

smaller industrial explosions, very near or at the earth's surface, would typically produce comparable, or even larger signals.)

V. Modeling High Frequency Seismic Noise: Atmospheric Sources

The nature of high frequency seismic noise is indicated by the observed noise acceleration power shown in Figure (15). The station shown (BAY) is near the former Soviet test site in Kazakh and is typical of the high frequency noise seen both within the former USSR and elsewhere. Three components of ground acceleration on the surface and at about 100 meters depth are shown. Both high and low wind level seismic noise spectra are shown on each plot. In all cases the high frequency seismic noise increases with high wind levels. It is also apparent that the acceleration power is roughly constant over the band from about 1 Hz to 30 Hz. Above 30 Hz the noise acceleration power decreases with increasing frequency, particularly in the bore-hole at 100m. depth.

Given the rather strong dependence of the noise level on wind velocity, it is natural to infer that atmospheric coupling at the earths surface is an important means of excitiation of high frequency seismic noise. A more detailed understanding of the atmospheric excitation of seismic noise is clearly important since the reduction or cancelation of this noise is dependent on an understanding of its origins, mode of excitation and propagation within the medium.

In order to investigate the production of seismic noise by atmospheric processes, the atmospheric modeling programs were linked with the linear elastic seismic modeling programs. The lower atmosphere, composed of a day-time turbulence boundary layer with a heigh of 2 km, is simulated with a random surface topography. Winds,

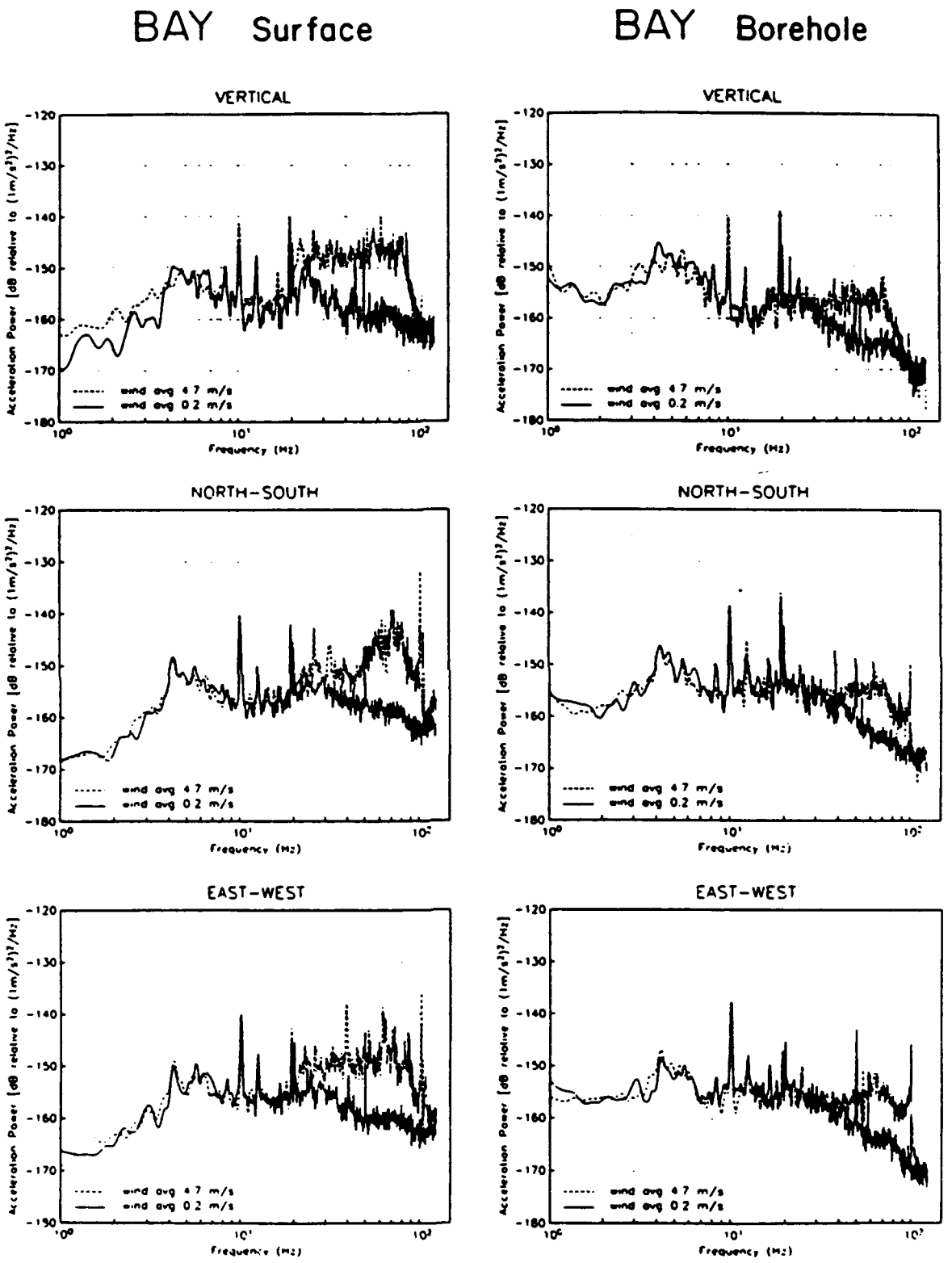

Figure (15.) Observed high frequency seismic noise acceleration power spectra at a site near the test site in Kazakh. Two wind level conditions are shown for sensors at the surface and at a depth of about 100m. (Data from Berger *et. al.*, 1989).

blowing on the topography, induce upward and downward flow velocities. Random temperature changes in space on the ground surface also produce flows that self-organize into plumes that coalesce above the boundary layer into larger scale thermals. Together with random turbulence in the boundary layer, these flows induce pressure and velocity fluctuations along the ground surface. These effects are the input into the seismic modeling code which integrates in time from the top-most surface boundary.

Preliminary results indicate that the seismic noise that is produced decreases in amplitude with depth and, as shown in Figure (16), produces a seismic velocity spectrum that has a trend that decreases as 1/f with increasing frequency, in the range from about 1 to 50Hz. Below about 40 meters the seismic noise appears to interact in such a manner that much smoother variations in spatial distributions are obtained than at the surface and with associated decreasing fluctuations in time. Both topography and winds are found to be of major importance in terms of amplitude and character of the noise. From preliminary results it can be expected that time of day will also be important due to the change of the turbulent boundary layer with the heating of the Sun and its temporal dependence.

VI. Summary and Conclusions

We have tested and modified our atmospheric modeling capabilities to include the most important non-linear effects, in particular the effects of sub-grid scale turbulence. We have made good progress on the turbulence phenomena by introducing a randomly fluctuating component to the field variables (i.e., pressure, velocites, temperature and density) that simulates sub-grid level turbulent effects. Results are encouraging and in particular give stable dynamical solutions to test problems that are comparable

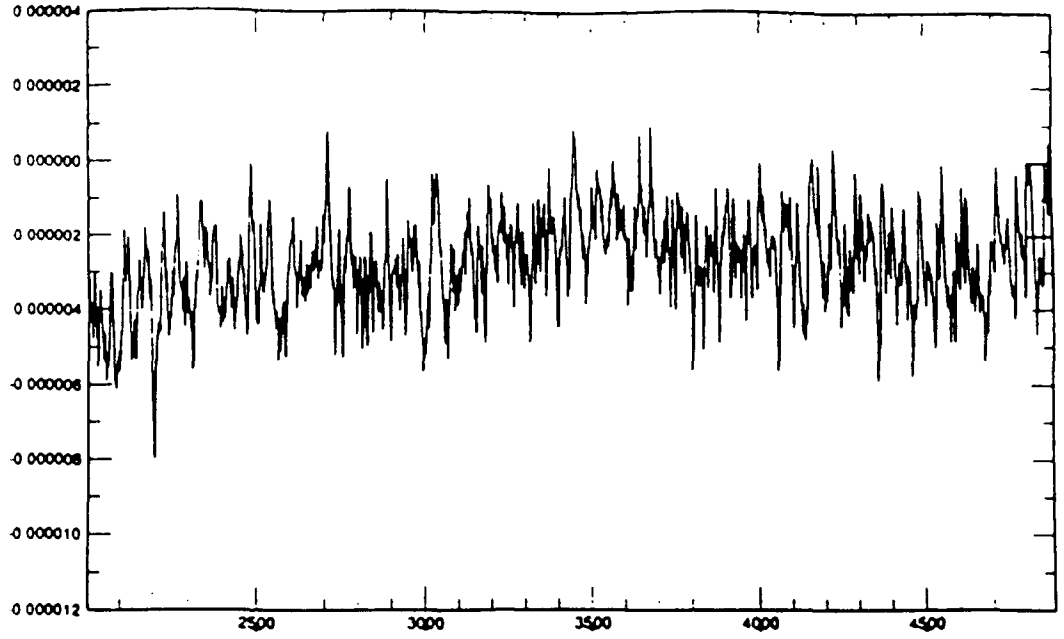

(a.) Seismic noise (velocity versus time) near the free surface due to the atmospheric turbulence.

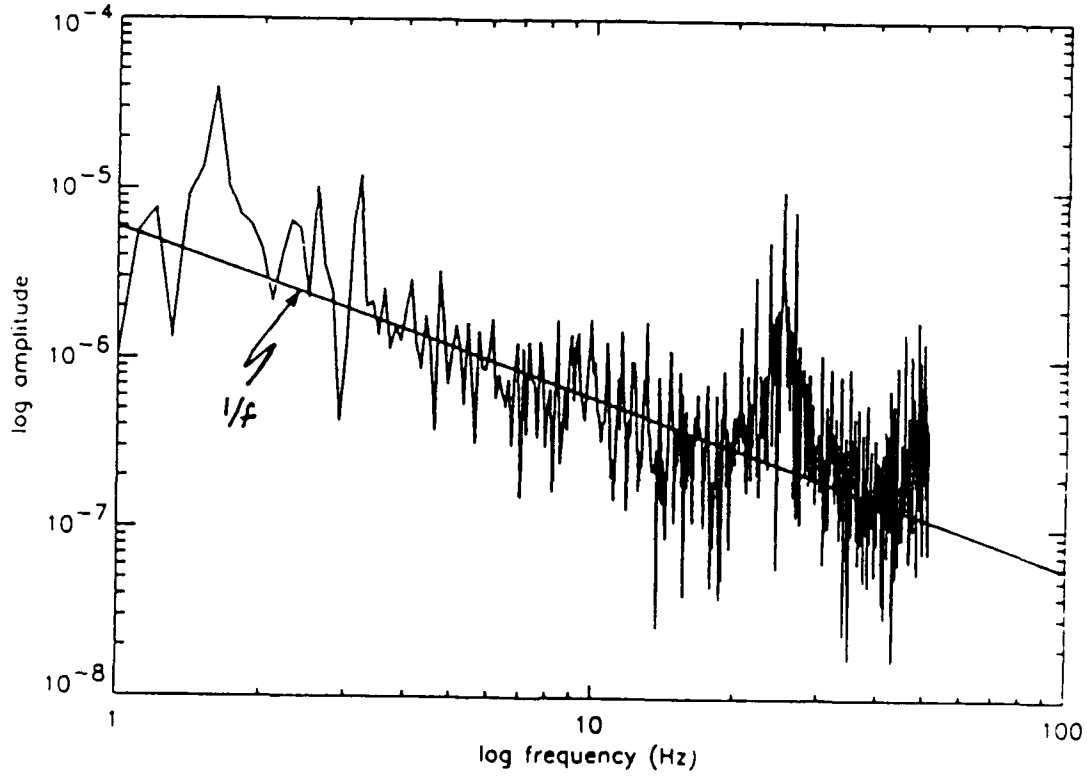

(b) Fourier spectrum of the seismic (velocity) noise in (a). The trend of the mean spectrum is as f^{-1}, which is what is commonly observed.

Figure (16). Theoretically predicted seismic noise due to models of atmospheric turbulence at the earth's free surface.

to observations.

The seismic investigations have focused on generation and testing of 2 and 3D finite difference programs that incorporate surface topography, medium randomness and lateral variability. Adaptation of FFT methods coupled with moving grids have been successful when tested against analytical and conventional finite difference methods and can, in principle, provide capabilities for predictions of wave fields in heterogenous media at regional distance ranges using moderate sized computers (e.g., high level work-stations such as the Stellar Computer) with only modest core size requirements (i.e., a few hundred megabytes). Transmitting grid boundaries have also been developed and tested with success. Analytical (modal) theory methods are being developed for 3D laterally varying media, to be used along with the 2D theory already developed.

Results of modeling studies and their comparisons with observed data have shown that:

(1) The atmospheric-ionospheric modeling predictions of electron density fluctuations have amplitudes and wave forms of the size and type inferred from observations.

(2) Coupled atmospheric-seismic modeling indicates that atmospheric turbulence, simulated by random fluctuations in state variables near the free surface, produces high frequency seismic noise with spectral character close to that observed; that is with a velocity amplitude spectrum varying as 1/f as a function of frequency above 1Hz.

(3) Seismic wave field modeling in complex structural models, incorporating rough, near source topography and fine scale randomized layering, produces seismic syn-

thetics having the complex character of observed seismograms. Simple vertical and horizontal randomization can only be an adequate representation of earth structure, and the seismic wave fields observed, within a few tens of wavelengths from the source. Beyond that distance the effects of strong shallow lateral variations in both average and random characteristics of the earth's structure produce effects in the observed wave field that become of first order and therefore important, so that accounting for large scale lateral variations is necessary to explain observed seismic wave fields in the regional distance range.

(4) Preliminary studies of particular complex seismic wave types, such as L_g and R_g, indicate that only large scale lateral variations in structure, in combination with both vertical and lateral randomization can explain the wave forms and attenuation characteristics observed.

Observational studies that have been a part of our investigations indicate that:

(5) High frequency seismic P waves (5-30Hz) propagate to considerable distances with high efficiency in stable continental areas. Direct observations indicate that the 20-30Hz band can be detected well above noise levels in this frequency range to distances of the order of 1000km. In tectonic regions the efficiency is lower, with signal energy in the 20-30Hz band generally detectable to about 400-500km.

(6) Quantitative investigations show that the geometric distance exponent is near -1 in stable continental areas and near -2 in tectonic areas. The dissipation function, Q, when constrained to be frequency independent in the 1-30Hz band, provides a fit to P wave spectral ratio data in both stable and tectonic continental areas of the former Soviet Union. We obtain values of between 3000 and 4000 for stable

areas and between 1000 to 2000 in tectonic areas.

In the future we plan to apply the modeling techniques developed in a wide range of more systematic studies and comparisons with observations, as well as to extend our domain of modeling capability to greater distance ranges and higher frequencies. Our ultimate objective will be to understand and predict phenomena under a variety of conditions involving medium structure and rheological behavior and to then devise source identification methods based on these results while testing them against both synthetic and observed data.

References

Berger, J., H.K. Givens, F.L. Vernon, I.L. Nersesov, M.B. Gokhberg, O.A. Stolyrov and N.T. Tarasov, Studies of High-Frequency Noise in Eastern Kazakhstan, *Bull. Seism. Soc. Am.* 1989.

Evernden, J.F., C.B. Archambeau and E. Cranwick, An Evaluation of Seismic Decoupling and Underground Nuclear Test Monitoring Using High Frequency Seismic Data, *Reviews of Geophysics, 24,* 143-215, May 1986.

Givens, H.K., N.T. Tarasov, V. Zharavlev, C.H. Thurber, F.L. Vernon, F. Berger and I.L. Nersesov, High Frequency Seismic Observations of Chemical Explosions of Known Location and Yield in Eastern Kazakhstan, USSR, *J.G.R.,* 1989.

Harvey, D.J. and R.A. Hansen, A Systematic Study of the Effects of Crust and Upper Mantle Structure on Regional Seismograms, Proceedings of the AFPL/DARPA Symposium on Nuclear Test Monitoring, Keystone Colorado, 1991.

Harvey, D.J., Seismogram Synthesis Using Normal Mode Superposition: The Locked Mode Approximation, *Geophys. J. R. Astr. Soc. 66,* pp. 37-61, 1981.

Kosloff, D., D. Kessler, A.Q. Filho, E. Tessmer, A. Behle, and R. Strahilevitz, Solution of the Equations of Dynamic Elasticity by a Chebychev Spectral Method, *Geophysic, vol. 55, no. 6,* June 1990, pp. 734-748.

Savino, J.M., C.B. Archambeau and J.F. Masso, VFM Discrimination Results from a Ten Station Network, *Systems, Science and Software Final Report: Air Force Technical Applications Center/Vela Seismological Center, USC-TR-81-29, 1980.*

Witte, D.C. and P.G. Richards, The Pseudospectral Method for Simulating Wave Propagation, *Computational Acoustics, 3,* 1990.

DISTRIBUTION LIST

Prof. Thomas Ahrens
Seismological Lab, 252-21
Division of Geological & Planetary Sciences
California Institute of Technology
Pasadena, CA 91125

Prof. Keiiti Aki
Center for Earth Sciences
University of Southern California
University Park
Los Angeles, CA 90089-0741

Prof. Shelton Alexander
Geosciences Department
403 Deike Building
The Pennsylvania State University
University Park, PA 16802

Dr. Ralph Alewine, III
DARPA/NMRO
3701 North Fairfax Drive
Arlington, VA 22203-1714

Prof. Charles B. Archambeau
CIRES
University of Colorado
Boulder, CO 80309

Dr. Thomas C. Bache, Jr.
Science Applications Int'l Corp.
10260 Campus Point Drive
San Diego, CA 92121 (2 copies)

Prof. Muawia Barazangi
Institute for the Study of the Continent
Cornell University
Ithaca, NY 14853

Dr. Jeff Barker
Department of Geological Sciences
State University of New York
at Binghamton
Vestal, NY 13901

Dr. Douglas R. Baumgardt
ENSCO, Inc
5400 Port Royal Road
Springfield, VA 22151-2388

Dr. Susan Beck
Department of Geosciences
Building #77
University of Arizona
Tuscon, AZ 85721

Dr. T.J. Bennett
S-CUBED
A Division of Maxwell Laboratories
11800 Sunrise Valley Drive, Suite 1212
Reston, VA 22091

Dr. Robert Blandford
AFTAC/TT, Center for Seismic Studies
1300 North 17th Street
Suite 1450
Arlington, VA 22209-2308

Dr. G.A. Bollinger
Department of Geological Sciences
Virginia Polytechnical Institute
21044 Derring Hall
Blacksburg, VA 24061

Dr. Stephen Bratt
Center for Seismic Studies
1300 North 17th Street
Suite 1450
Arlington, VA 22209-2308

Dr. Lawrence Burdick
Woodward-Clyde Consultants
566 El Dorado Street
Pasadena, CA 91109-3245

Dr. Robert Burridge
Schlumberger-Doll Research Center
Old Quarry Road
Ridgefield, CT 06877

Dr. Jerry Carter
Center for Seismic Studies
1300 North 17th Street
Suite 1450
Arlington, VA 22209-2308

Dr. Eric Chael
Division 9241
Sandia Laboratory
Albuquerque, NM 87185

Prof. Vernon F. Cormier
Department of Geology & Geophysics
U-45, Room 207
University of Connecticut
Storrs, CT 06268

Prof. Steven Day
Department of Geological Sciences
San Diego State University
San Diego, CA 92182

Marvin Denny
U.S. Department of Energy
Office of Arms Control
Washington, DC 20585

Dr. Zoltan Der
ENSCO, Inc.
5400 Port Royal Road
Springfield, VA 22151-2388

Prof. Adam Dziewonski
Hoffman Laboratory, Harvard University
Dept. of Earth Atmos. & Planetary Sciences
20 Oxford Street
Cambridge, MA 02138

Prof. John Ebel
Department of Geology & Geophysics
Boston College
Chestnut Hill, MA 02167

Eric Fielding
SNEE Hall
INSTOC
Cornell University
Ithaca, NY 14853

Dr. Mark D. Fisk
Mission Research Corporation
735 State Street
P.O. Drawer 719
Santa Barbara, CA 93102

Prof Stanley Flatte
Applied Sciences Building
University of California, Santa Cruz
Santa Cruz, CA 95064

Dr. John Foley
NER-Geo Sciences
1100 Crown Colony Drive
Quincy, MA 02169

Prof. Donald Forsyth
Department of Geological Sciences
Brown University
Providence, RI 02912

Dr. Art Frankel
U.S. Geological Survey
922 National Center
Reston, VA 22092

Dr. Cliff Frolich
Institute of Geophysics
8701 North Mopac
Austin, TX 78759

Dr. Holly Given
IGPP, A-025
Scripps Institute of Oceanography
University of California, San Diego
La Jolla, CA 92093

Dr. Jeffrey W. Given
SAIC
10260 Campus Point Drive
San Diego, CA 92121

Dr. Dale Glover
Defense Intelligence Agency
ATTN: ODT-1B
Washington, DC 20301

Dr. Indra Gupta
Teledyne Geotech
314 Montgomery Street
Alexanderia, VA 22314

Dan N. Hagedon
Pacific Northwest Laboratories
Battelle Boulevard
Richland, WA 99352

Dr. James Hannon
Lawrence Livermore National Laboratory
P.O. Box 808
L-205
Livermore, CA 94550

Dr. Roger Hansen
HQ AFTAC/TTR
Patrick AFB, FL 32925-6001

Prof. David G. Harkrider
Seismological Laboratory
Division of Geological & Planetary Sciences
California Institute of Technology
Pasadena, CA 91125

Prof. Danny Harvey
CIRES
University of Colorado
Boulder, CO 80309

Prof. Donald V. Helmberger
Seismological Laboratory
Division of Geological & Planetary Sciences
California Institute of Technology
Pasadena, CA 91125

Prof. Eugene Herrin
Institute for the Study of Earth and Man
Geophysical Laboratory
Southern Methodist University
Dallas, TX 75275

Prof. Robert B. Herrmann
Department of Earth & Atmospheric Sciences
St. Louis University
St. Louis, MO 63156

Prof. Lane R. Johnson
Seismographic Station
University of California
Berkeley, CA 94720

Prof. Thomas H. Jordan
Department of Earth, Atmospheric &
Planetary Sciences
Massachusetts Institute of Technology
Cambridge, MA 02139

Prof. Alan Kafka
Department of Geology & Geophysics
Boston College
Chestnut Hill, MA 02167

Robert C. Kemerait
ENSCO, Inc.
445 Pineda Court
Melbourne, FL 32940

Dr. Max Koontz
U.S. Dept. of Energy/DP 5
Forrestal Building
1000 Independence Avenue
Washington, DC 20585

Dr. Richard LaCoss
MIT Lincoln Laboratory, M-200B
P.O. Box 73
Lexington, MA 02173-0073

Dr. Fred K. Lamb
University of Illinois at Urbana-Champaign
Department of Physics
1110 West Green Street
Urbana, IL 61801

Prof. Charles A. Langston
Geosciences Department
403 Deike Building
The Pennsylvania State University
University Park, PA 16802

Jim Lawson, Chief Geophysicist
Oklahoma Geological Survey
Oklahoma Geophysical Observatory
P.O. Box 8
Leonard, OK 74043-0008

Prof. Thorne Lay
Institute of Tectonics
Earth Science Board
University of California, Santa Cruz
Santa Cruz, CA 95064

Dr. William Leith
U.S. Geological Survey
Mail Stop 928
Reston, VA 22092

Mr. James F. Lewkowicz
Phillips Laboratory/GPEH
Hanscom AFB, MA 01731-5000(2 copies)

Mr. Alfred Lieberman
ACDA/VI-OA State Department Building
Room 5726
320-21st Street, NW
Washington, DC 20451

Prof. L. Timothy Long
School of Geophysical Sciences
Georgia Institute of Technology
Atlanta, GA 30332

Dr. Randolph Martin, III
New England Research, Inc.
76 Olcott Drive
White River Junction, VT 05001

Dr. Robert Masse
Denver Federal Building
Box 25046, Mail Stop 967
Denver, CO 80225

Dr. Gary McCartor
Department of Physics
Southern Methodist University
Dallas, TX 75275

Prof. Thomas V. McEvilly
Seismographic Station
University of California
Berkeley, CA 94720

Dr. Art McGarr
U.S. Geological Survey
Mail Stop 977
U.S. Geological Survey
Menlo Park, CA 94025

Dr. Keith L. McLaughlin
S-CUBED
A Division of Maxwell Laboratory
P.O. Box 1620
La Jolla, CA 92038-1620

Stephen Miller & Dr. Alexander Florence
SRI International
333 Ravenswood Avenue
Box AF 116
Menlo Park, CA 94025-3493

Prof. Bernard Minster
IGPP, A-025
Scripps Institute of Oceanography
University of California, San Diego
La Jolla, CA 92093

Prof. Brian J. Mitchell
Department of Earth & Atmospheric Sciences
St. Louis University
St. Louis, MO 63156

Mr. Jack Murphy
S-CUBED
A Division of Maxwell Laboratory
11800 Sunrise Valley Drive, Suite 1212
Reston, VA 22091 (2 Copies)

Dr. Keith K. Nakanishi
Lawrence Livermore National Laboratory
L-025
P.O. Box 808
Livermore, CA 94550

Dr. Carl Newton
Los Alamos National Laboratory
P.O. Box 1663
Mail Stop C335, Group ESS-3
Los Alamos, NM 87545

Dr. Bao Nguyen
HQ AFTAC/TTR
Patrick AFB, FL 32925-6001

Prof. John A. Orcutt
IGPP, A-025
Scripps Institute of Oceanography
University of California, San Diego
La Jolla, CA 92093

Prof. Jeffrey Park
Kline Geology Laboratory
P.O. Box 6666
New Haven, CT 06511-8130

Dr. Howard Patton
Lawrence Livermore National Laboratory
L-025
P.O. Box 808
Livermore, CA 94550

Dr. Frank Pilotte
HQ AFTAC/TT
Patrick AFB, FL 32925-6001

Dr. Jay J. Pulli
Radix Systems, Inc.
2 Taft Court, Suite 203
Rockville, MD 20850

Dr. Robert Reinke
ATTN: FCTVTD
Field Command
Defense Nuclear Agency
Kirtland AFB, NM 87115

Prof. Paul G. Richards
Lamont-Doherty Geological Observatory
of Columbia University
Palisades, NY 10964

Mr. Wilmer Rivers
Teledyne Geotech
314 Montgomery Street
Alexandria, VA 22314

Dr. George Rothe
HQ AFTAC/TTR
Patrick AFB, FL 32925-6001

Dr. Alan S. Ryall, Jr.
DARPA/NMRO
3701 North Fairfax Drive
Arlington, VA 22209-1714

Dr. Richard Sailor
TASC, Inc.
55 Walkers Brook Drive
Reading, MA 01867

Prof. Charles G. Sammis
Center for Earth Sciences
University of Southern California
University Park
Los Angeles, CA 90089-0741

Prof. Christopher H. Scholz
Lamont-Doherty Geological Observatory
of Columbia University
Palisades, CA 10964

Dr. Susan Schwartz
Institute of Tectonics
1156 High Street
Santa Cruz, CA 95064

Secretary of the Air Force
(SAFRD)
Washington, DC 20330

Office of the Secretary of Defense
DDR&E
Washington, DC 20330

Thomas J. Sereno, Jr.
Science Application Int'l Corp.
10260 Campus Point Drive
San Diego, CA 92121

Dr. Michael Shore
Defense Nuclear Agency/SPSS
6801 Telegraph Road
Alexandria, VA 22310

Dr. Matthew Sibol
Virginia Tech
Seismological Observatory
4044 Derring Hall
Blacksburg, VA 24061-0420

Prof. David G. Simpson
IRIS, Inc.
1616 North Fort Myer Drive
Suite 1440
Arlington, VA 22209

Donald L. Springer
Lawrence Livermore National Laboratory
L-025
P.O. Box 808
Livermore, CA 94550

Dr. Jeffrey Stevens
S-CUBED
A Division of Maxwell Laboratory
P.O. Box 1620
La Jolla, CA 92038-1620

Lt. Col. Jim Stobie
ATTN: AFOSR/NL
Bolling AFB
Washington, DC 20332-6448

Prof. Brian Stump
Institute for the Study of Earth & Man
Geophysical Laboratory
Southern Methodist University
Dallas, TX 75275

Prof. Jeremiah Sullivan
University of Illinois at Urbana-Champaign
Department of Physics
1110 West Green Street
Urbana, IL 61801

Prof. L. Sykes
Lamont-Doherty Geological Observatory
of Columbia University
Palisades, NY 10964

Dr. David Taylor
ENSCO, Inc.
445 Pineda Court
Melbourne, FL 32940

Dr. Steven R. Taylor
Los Alamos National Laboratory
P.O. Box 1663
Mail Stop C335
Los Alamos, NM 87545

Prof. Clifford Thurber
University of Wisconsin-Madison
Department of Geology & Geophysics
1215 West Dayton Street
Madison, WS 53706

Prof. M. Nafi Toksoz
Earth Resources Lab
Massachusetts Institute of Technology
42 Carleton Street
Cambridge, MA 02142

Dr. Larry Turnbull
CIA-OSWR/NED
Washington, DC 20505

Dr. Gregory van der Vink
IRIS, Inc.
1616 North Fort Myer Drive
Suite 1440
Arlington, VA 22209

Dr. Karl Veith
EG&G
5211 Auth Road
Suite 240
Suitland, MD 20746

Prof. Terry C. Wallace
Department of Geosciences
Building #77
University of Arizona
Tuscon, AZ 85721

Dr. Thomas Weaver
Los Alamos National Laboratory
P.O. Box 1663
Mail Stop C335
Los Alamos, NM 87545

Dr. William Wortman
Mission Research Corporation
8560 Cinderbed Road
Suite 700
Newington, VA 22122

Prof. Francis T. Wu
Department of Geological Sciences
State University of New York
at Binghamton
Vestal, NY 13901

AFTAC/CA
(STINFO)
Patrick AFB, FL 32925-6001

DARPA/PM
3701 North Fairfax Drive
Arlington, VA 22203-1714

DARPA/RMO/RETRIEVAL
3701 North Fairfax Drive
Arlington, VA 22203-1714

DARPA/RMO/SECURITY OFFICE
3701 North Fairfax Drive
Arlington, VA 22203-1714

HQ DNA
ATTN: Technical Library
Washington, DC 20305

Defense Intelligence Agency
Directorate for Scientific & Technical Intelligence
ATTN: DTIB
Washington, DC 20340-6158

Defense Technical Information Center
Cameron Station
Alexandria, VA 22314 (2 Copies)

TACTEC
Battelle Memorial Institute
505 King Avenue
Columbus, OH 43201 (Final Report)

Phillips Laboratory
ATTN: XPG
Hanscom AFB, MA 01731-5000

Phillips Laboratory
ATTN: GPE
Hanscom AFB, MA 01731-5000

Phillips Laboratory
ATTN: TSML
Hanscom AFB, MA 01731-5000

Phillips Laboratory
ATTN: SUL
Kirtland, NM 87117 (2 copies)

Dr. Michel Bouchon
I.R.I.G.M.-B.P. 68
38402 St. Martin D'Heres
Cedex, FRANCE

Dr. Michel Campillo
Observatoire de Grenoble
I.R.I.G.M.-B.P. 53
38041 Grenoble, FRANCE

Dr. Kin Yip Chun
Geophysics Division
Physics Department
University of Toronto
Ontario, CANADA

Prof. Hans-Peter Harjes
Institute for Geophysic
Ruhr University/Bochum
P.O. Box 102148
4630 Bochum 1, GERMANY

Prof. Eystein Husebye
NTNF/NORSAR
P.O. Box 51
N-2007 Kjeller, NORWAY

David Jepsen
Acting Head, Nuclear Monitoring Section
Bureau of Mineral Resources
Geology and Geophysics
G.P.O. Box 378, Canberra, AUSTRALIA

Ms. Eva Johannisson
Senior Research Officer
National Defense Research Inst.
P.O. Box 27322
S-102 54 Stockholm, SWEDEN

Dr. Peter Marshall
Procurement Executive
Ministry of Defense
Blacknest, Brimpton
Reading FG7-FRS, UNITED KINGDOM

Dr. Bernard Massinon, Dr. Pierre Mechler
Societe Radiomana
27 rue Claude Bernard
75005 Paris, FRANCE (2 Copies)

Dr. Svein Mykkeltveit
NTNT/NORSAR
P.O. Box 51
N-2007 Kjeller, NORWAY (3 Copies)

Prof. Keith Priestley
University of Cambridge
Bullard Labs, Dept. of Earth Sciences
Madingley Rise, Madingley Road
Cambridge CB3 OEZ, ENGLAND

Dr. Jorg Schlittenhardt
Federal Institute for Geosciences & Nat'l Res.
Postfach 510153
D-3000 Hannover 51, GERMANY

Dr. Johannes Schweitzer
Institute of Geophysics
Ruhr University/Bochum
P.O. Box 1102148
4360 Bochum 1, GERMANY